Cell

MicroRNA Directly Enhances Mitochondrial Translation during Muscle Differentiation

Xiaorong Zhang,[1] Xinxin Zuo,[1] Bo Yang,[1] Zongran Li,[1] Yuanchao Xue,[1,2] Yu Zhou,[2] Jie Huang,[1] Xiaolu Zhao,[1] Jie Zhou,[1] Yun Yan,[1] Huiqiong Zhang,[1] Peipei Guo,[1] Hui Sun,[1] Lin Guo,[1] Yi Zhang,[1,4] and Xiang-Dong Fu[1,2,3,*]
[1]State Key Laboratory of Virology, College of Life Sciences, Wuhan University, Wuhan, Hubei 430072, China
[2]Department of Cellular and Molecular Medicine
[3]Institute of Genomic Medicine
University of California, San Diego, La Jolla, CA 92093-0651, USA
[4]Present address: Center for Genome Analysis, ABLife Inc., Novonest Building 135, 8 Nanhu Avenue, East Lake Hi-Tech Development Zone, Wuhan, Hubei 430079, China
*Correspondence: xdfu@ucsd.edu
http://dx.doi.org/10.1016/j.cell.2014.05.047

SUMMARY

MicroRNAs are well known to mediate translational repression and mRNA degradation in the cytoplasm. Various microRNAs have also been detected in membrane-compartmentalized organelles, but the functional significance has remained elusive. Here, we report that miR-1, a microRNA specifically induced during myogenesis, efficiently enters the mitochondria where it unexpectedly stimulates, rather than represses, the translation of specific mitochondrial genome-encoded transcripts. We show that this positive effect requires specific miR:mRNA base-pairing and Ago2, but not its functional partner GW182, which is excluded from the mitochondria. We provide evidence for the direct action of Ago2 in mitochondrial translation by crosslinking immunoprecipitation coupled with deep sequencing (CLIP-seq), functional rescue with mitochondria-targeted Ago2, and selective inhibition of the microRNA machinery in the cytoplasm. These findings unveil a positive function of microRNA in mitochondrial translation and suggest a highly coordinated myogenic program via miR-1-mediated translational stimulation in the mitochondria and repression in the cytoplasm.

INTRODUCTION

The function and mechanism of microRNAs (miRNAs) have been well studied in higher eukaryotic cells. miRNAs bind their target mRNAs via partial base-pairing within the RNA-induced silencing complexes (RISC) and regulate both mRNA stability and translation (Carthew and Sontheimer, 2009; Chekulaeva and Filipowicz, 2009). miRNA-mediated RNA degradation can be accomplished via a slicing-competent Ago protein (Ago2 in mammals) to cleave target mRNA in the mRNA:miRNA duplex. The broad function of RISC in translational control is mediated by the key Ago partner GW182 to recruit deadenylating/decapping enzymes to allow exonucleases to attack unprotected mRNA and repress translation through competing with the cap binding protein eIF4E and/or interfering with ribosome scanning (Czech and Hannon, 2011).

Besides their primary functions in translational repression, miRNAs have also been implicated in enhancing translation under specific cellular conditions (Vasudevan, 2012). This was first observed in serum-starved cells (Vasudevan et al., 2007), but such an opposite function of miRNAs has not been widely appreciated, partly because the potential mechanism involved has remained largely unclear. Biochemical experiments with fly extracts provided some initial hint to this unconventional miRNA function, showing that a target mRNA lacking both cap and typical poly(A) tail permits enhanced translation when the miRNA is assembled into a complex with a GW182-detached Ago protein (Iwasaki and Tomari, 2009). Related phenomena have also been observed in immature oocytes where the miRNA machinery is either in an inactive state (Suh et al., 2010) or even stimulates translation of target transcripts (Mortensen et al., 2011).

The miRNA machinery is known to primarily act in the cytoplasm. However, growing evidence suggests that both miRNAs and proteins of the Argonaute family also play important roles in transcriptional control (Cernilogar et al., 2011; Guang et al., 2008) and DNA repair (Wei et al., 2012). miRNAs have also been detected in membrane-bound compartments, such as secreted vesicles (Zhang et al., 2010) and mitochondria (Bandiera et al., 2011; Barrey et al., 2011; Das et al., 2012; Kren et al., 2009; Sripada et al., 2012). The presence of miRNAs in the mitochondria is somewhat surprising because mitochondria maintain their own genome, and in many aspects, resemble bacteria (Taanman, 1999); however, the functional significance of miRNAs in the mitochondria has remained largely unknown. One report indicates that miR-181c could repress the translation of a mitochondrial transcript, but paradoxically, reduced translation led

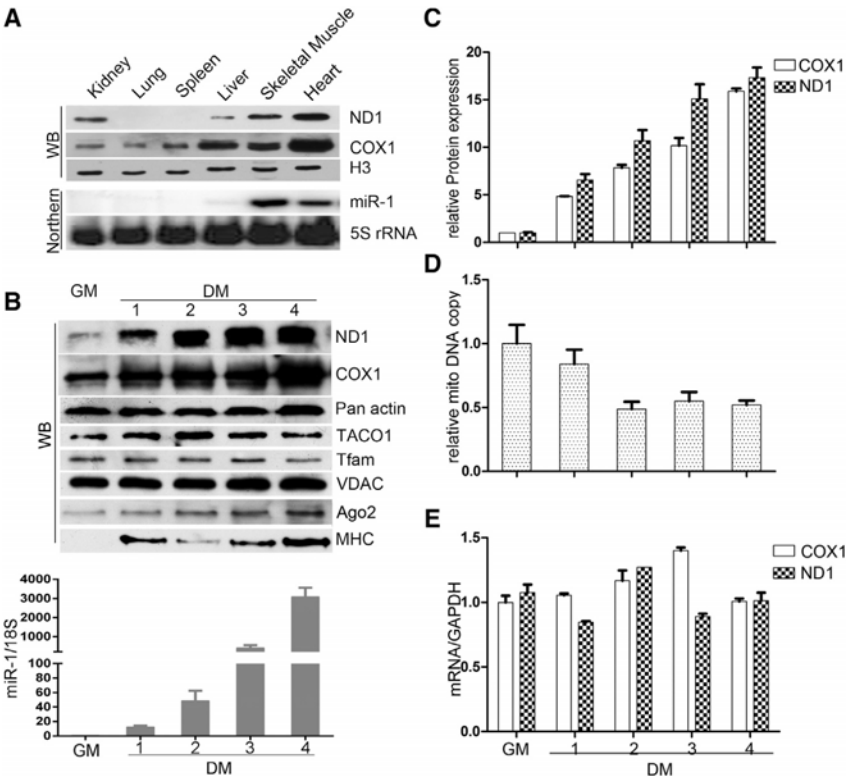

Figure 1. Increased Mitochondrial Proteins without a Significant Elevation in mtDNA Copy Number or Transcription

(A) Levels of COX1 and ND1 proteins detected by western blotting and miR-1 by Northern blotting in different adult mouse tissues. Levels of Histone H3 and 5S rRNA served as protein and RNA loading controls, respectively.

(B) Western and TaqMan PCR analysis of COX1, ND1, and miR-1 in C2C12 cells before and after differentiation. Pan actin and VDAC served as protein loading controls and 28S rRNA as an RNA loading control. MHC was analyzed as a control for the induction of the myogenic program. Tfam and TACO1 were analyzed to detect potential regulation of critical mitochondrial transcriptional and translational regulators.

(C–E) Quantification of proteins normalized to pan actin (C), mtDNA normalized to nuclear DNA (D), and RNA normalized to GAPDH, (E) during C2C12 cell differentiation. Data in (C) and (E) are based on three biological repeats and data in (D) on ten biological repeats. Errors bars are mean ± SD.

See also Figure S1.

to an overall enhancement of mitochondrial activities in ventricular myocytes (Das et al., 2012).

Our current study was initially geared to investigate a puzzle that mitochondrial DNA (mtDNA)-encoded proteins were greatly elevated during muscle differentiation, but without a significant increase in mtDNA copy number or transcription. This leads to an unexpected finding that the muscle-specific miR-1 is able to stimulate mitochondrial translation of multiple mtDNA-encoded transcripts, while repressing its nuclear DNA-encoded targets in the cytoplasm. Such a miRNA-dependent effect requires Ago2, but not its normal functional partner GW182, consistent with the presence of a significant amount of Ago2, but not GW182, in the mitochondria. These findings provide critical insights into miRNA action mechanisms, functional conservation of the Argonaute family of proteins in diverse organisms, change in bioenergetics mechanisms during cell differentiation, and the regulation of mitochondrial translation in higher eukaryotic cells.

RESULTS

Marked Increase in Mitochondrial Protein Synthesis during Muscle Differentiation

Mitochondria generate ATP through oxidative phosphorylation to provide the chemical form of energy for cellular activities (Saraste, 1999). The energy demand is especially high in cardiac and skeletal muscle (Lopaschuk et al., 2010; Moyes et al., 1997). Consistently, we detected much higher levels of mtDNA-encoded proteins in muscle cells relative to constant amounts of nuclear DNA-encoded histone H3 protein and 5S rRNA in different mouse tissues (Figure 1A). Such a marked increase was also evident during C2C12 cell differentiation from myoblasts to myotubes, characterized by the induction of the myosin heavy chain (MHC) and the muscle-specific miRNA miR-1 (Chen et al., 2006; Rao et al., 2006). However, both actin and the nuclear DNA-encoded, mitochondrial residential protein VDAC were constant (Figure 1B). Quantitative analysis indicates that the mitochondrial ND1 and COX1 proteins were increased by more than 15-fold during C2C12 cell differentiation (Figure 1C).

Significantly, such a dramatic elevation in protein synthesis was not accompanied by mtDNA replication during C2C12 cell differentiation (Figure 1D), as reported earlier (Franko et al., 2008). The mRNA levels for both COX1 and ND1 were also invariant (Figure 1E), which was further confirmed by RT-qPCR with three distinct primer sets (Figure S1 available online). This is consistent with little change in TFAM expression (Figure 1B), a vital transcriptional activator in the mitochondria (Bestwick and Shadel, 2013). Because we did not detect any induction of TACO1 (Figure 1B), a major translational activator for COX1 (Weraarpachai et al., 2009), these data suggest a previously unknown mechanism that may account for induced mitochondrial translation during muscle differentiation.

Evidence for the Presence of Ago2 within the Mitochondria

Given the recent observations that various miRNAs were detected in isolated mitochondria from rat liver (Kren et al., 2009), rat ventricular myocytes (Das et al., 2012), and several common human cell lines (Sripada et al., 2012), we reasoned that reduced miRNA targeting to the mitochondria might account for increased translation in the mitochondria during muscle

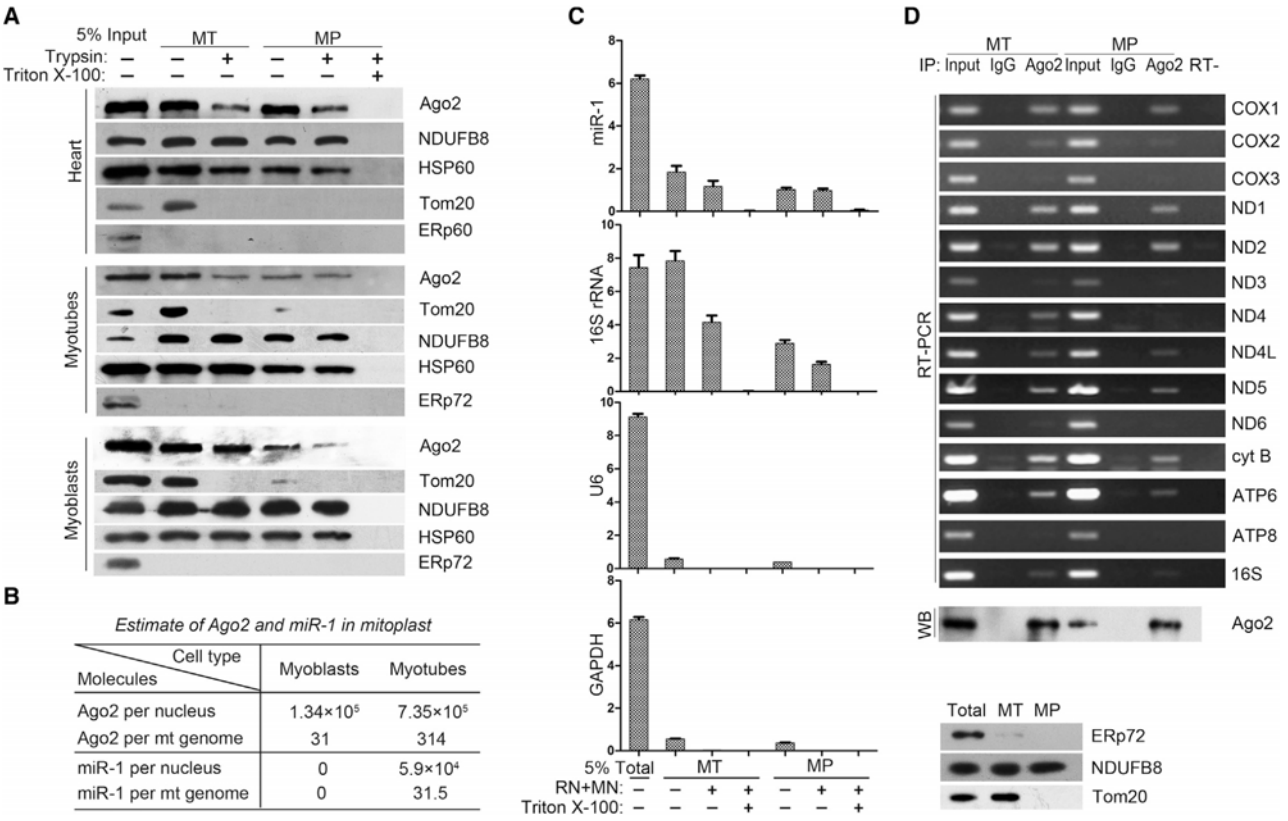

Figure 2. Detection and Quantitative Analysis of Ago2 and miR-1 in the Mitochondria

(A) Trypsin protection analysis of purified mitochondria (MT) and mitoplasts (MP) from adult mouse heart, C2C12 myoblasts, and C2C12 myotubes. See also Figure S2A.

(B) Quantification of Ago2 and miR-1 per C2C12 nucleus or per mitochondrial genome. The average number is based on two independent experiments. See also Figures S2C and S2D.

(C) Nuclease protection analysis. Three aliquots of purified mitochondria and mitoplasts were treated with isolation buffer, with RNase T1 (RN) plus MNase (MN), or with the combination of nucleases in the presence of Triton X-100. Data are based on triplicated experiments and error bars are means ± SD.

(D) Purified mitochondria and mitoplasts from the same fractionation experiment were first characterized by the lack of the ER marker ERp72, but the presence of outer membrane protein marker Tom20 in the mitochondria and the inner membrane marker NDUFB8 in both mitochondria and mitoplasts (bottom). Equal amounts of purified mitochondria and mitoplasts based on the levels of 16S rRNA were subjected to ribo-IP with anti-Ago2 or control IgG (top). Western blotting data showed specific anti-Ago2 IP. Individual mitochondrial transcripts were examined by semiquantitative RT-PCR.

See also Figures S2E and S2F for real-time RT-PCR analysis of Ago2-associated mitochondrial transcripts from purified mitoplasts.

differentiation. Alternatively, enhanced mitochondrial translation may indirectly result from repression of some nuclear DNA-encoded mitochondrial translational repressors, in line with the induction of Ago2 expression during C2C12 differentiation (Figure 1B).

To begin to explore these possibilities, we first used highly purified mitochondria to rigorously demonstrate that a fraction of Ago2 is indeed present within the mitochondria. Because purified mitochondria are often contaminated with endoplasmic reticulum (ER) proteins due to the intimate association between ER and the mitochondria (de Brito and Scorrano, 2008; Rizzuto et al., 1998), we selectively removed the outer membrane by treating purified mitochondria (MT) with digitonin to prepare mitoplasts (MP) from mouse heart or C2C12 cells before and after differentiation (Bosmann et al., 1972; Schnaitman and Greenawalt, 1968). We found that our initially purified mitochondria were largely free of ER contamination as indicated by the absence of the ER-specific protein ERp60 or ERp72 (Figure 2A). Upon digitonin treatment followed by sedimentation or fractionation on a sucrose gradient, the outer membrane was removed, as evidenced by the lack of Tom20, but the inner membrane was largely intact, as indicated by the presence of the inner membrane marker NDUFB8 and the mitochondrial matrix protein HSP60 (Figures 2A and S2A).

Under these rigorously controlled conditions, we detected Ago2 in both highly purified MT and MP, which became Trypsin-sensitive only when the inner membrane was further permeabilized with Triton X-100. Neither Ago1 nor Ago3 was detectable in MT and MP (Figure S2A), indicating that Ago2 may be selectively imported into the mitochondria. Tandem mass spectrometric analysis confirmed the identity of Ago2 immunoprecipitated from MP (Figure S2B). These data agree with the recent confocal microscopic result (Bandiera et al., 2011) and provide

the strongest biochemical evidence to date for the presence of Ago2 inside the mitochondria.

Quantification of Ago2 in the Mitochondria during Muscle Differentiation

We next wished to quantitatively determine the levels of Ago2 in the mitochondria during C2C12 cell differentiation by using the standard curve generated with Ago2 expressed in insect cells (Figures S2C and S2D). Because induced myotubes contain more than one nucleus, we determined the copy number of nuclear DNA by qPCR to calculate the number of Ago2 molecules per nuclear genome. This revealed 1.34×10^5 and 7.35×10^5 Ago2 molecules in C2C12 myoblasts and myotubes, respectively (Figure 2B), which is similar to the recent estimate of 1.4×10^5–1.7×10^5 Ago2 per cell on a human melanoma cell line (Wang et al., 2012).

We then determined the amount of Ago2 within the mitochondria by using mtDNA as an internal control (the copy number of mtDNA varies from 0 to 11 per mitochondria with the average = 2) (see Cavelier et al., 2000), which is necessary because of potential damage during MP preparation. This analysis revealed 31 and 314 Ago2 molecules, respectively, per mtDNA in C2C12 cells before and after differentiation (Figure 2B). We also determined the ratio of mitochondrial and nuclear DNA in our cellular system, revealing a ratio of 554 in myoblasts and 774 in myotubes, thus suggesting the presence of $31 \times 554/1.34 \times 10^5 = 12.8\%$ and $314 \times 774/7.35 \times 10^5 = 33.1\%$ of total cellular Ago2 in the mitochondria of C2C12 cells before and after differentiation, respectively. These quantitative data suggest that more Ago2 is targeted to the mitochondria upon C2C12 differentiation into myotubes.

Efficient Entry of Induced miR-1 into the Mitochondria of Muscle Cells

We similarly analyzed the quantity of miR-1 in the mitochondria by using highly purified mitoplasts, finding that a fraction of the newly induced miR-1 was indeed detectable inside the mitochondria of myotubes, which became sensitive to nuclease only in the presence of Triton X-100 (Figure 2C). The nuclease sensitivity of miR-1 was similar to the mitochondrial 16S rRNA. In contrast, both nuclear U6 small nuclear RNA (snRNA) and cytoplasmic GAPDH mRNA were largely removed from purified MT and MP, and any residual amounts could be fully degraded by a combination of RNase T1 (RN) and Micrococcal nuclease (MN) in the absence of detergent (Figure 2C). We further showed that our mitoplasts were highly purified away from the abundant 7SK noncoding RNA and multiple nuclear DNA-transcribed mRNAs for mitochondrial residential proteins (e.g., NDUFB8, COX4V1, and NDUFV1) (Figure S2E).

Using the same quantification strategy for Ago2, we determined the amount of miR-1 in the mitochondria, revealing 5.9×10^4 miR-1 per nuclear genome in myotubes (note that miR-1 was not detectable in myoblasts), 31.5 per mtDNA, and a total amount of $31.5 \times 775/5.9 \times 10^4 = 41.4\%$ in the mitochondria. Therefore, similar to Ago2, miR-1 is not only present in the mitochondria in a substantial quantity, but also increased, rather than decreased, during muscle cell differentiation.

Having thoroughly demonstrated the presence of both Ago2 and miR-1 in the mitochondria, we next performed Ribo-IP to determine whether Ago2 is associated with mitochondrial transcripts. Using consecutively purified MT and MP (characterized in the bottom of Figure 2D) from the same cell population, we found that anti-Ago2, but not control IgG, efficiently captured multiple mitochondrial transcripts (Figure 2D, top). These semi-quantitative results were further conformed by RT-qPCR with RNA recovered from purified mitoplasts (Figure S2F). Therefore, in contrast to our initial expectation, the miRNA machinery appears to become increased, rather than decreased, in the mitochondria of differentiated C2C12 cells.

Identification of Specific miR-1 Targets in C2C12 Cells

To determine specific targets for Ago2 and miR-1, we first designed a miRACE strategy to experimentally identify specific miRNA targets (Figure S3A), instead of relying on computational prediction, which is analogous to a published method (Easow et al., 2007). In this procedure, miRNA:mRNA duplexes were captured from whole-cell extracts with anti-Ago2 followed by in situ extension of endogenous miRNA into target mRNA with reverse transcriptase. The extended products were poly(C)-tailed at the 3′ end and PCR-amplified using a common primer linked to a poly(G) sequence and a miRNA-specific primer. While we are still refining this method for high-throughput analysis, we initially focused on identifying miR-1 targets by cloning and sequencing a sizable number of PCR products. This revealed that several cytoplasmic targets for miR-1, one of which (ELL2) was further validated (see below). Importantly, we identified multiple mitochondrial transcripts for this miRNA (Figure S3B).

The second approach we took was to map specific Ago2 binding events by crosslinking immunoprecipitation coupled with deep sequencing (CLIP-seq). We performed duplicated CLIP-seq on C2C12 myoblasts and myotubes, obtaining ~10 million uniquely mapped tags from each CLIP-seq library, which showed high concordance within the same cell types and large differences between the two cell types (Figure S3C). Compiling the normalized Ago2 binding events (to 1 million) on potential miR-1 cytoplasmic targets predicted by the miRNA target prediction program PITA (Kertesz et al., 2007), we observed no enrichment on myoblasts, but significant enrichment on myotubes, consistent with induced miR-1 only in myotubes (Figure 3A). Of five most characterized cytoplasmic miR-1 targets reported in the literature, four showed a dramatic increase in Ago2 binding on the target sites (Figure 3B). HDAC4 exhibited an Ago2 peak before C2C12 differentiation, indicative of the involvement of another miRNA(s), but the Ago2 level was further enhanced after C2C12 differentiation (Figure 3B). Together, these data demonstrated the robustness of our CLIP-seq data in pinpointing specific miRNA targeting sites in the nuclear genome.

Critical Insights from Mapped Ago2-RNA Interactions in the Mitochondria

We then turned our attention to Ago2 interaction with the mitochondrial genome. Because the nuclear genome is populated with multiple mitochondrial pseudogenes, we took extra caution in mapping CLIP-seq tags to mtDNA by dividing the CLIP-seq

tags into three classes that were (1) uniquely mapped to mitochondrial transcripts from mtDNA, (2) uniquely mapped to mitochondrial pseudogenes in the nuclear genome, and (3) commonly mapped to both nuclear and mitochondrial genomes (Table S1). This analysis revealed that the number of tags uniquely mapped to the nuclear mitochondrial pseudogenes is largely negligible. We therefore combined tags from class 1 and 3 (Table S2) to generate an Ago2 interaction map in the mitochondria. Significantly, we observed dramatic induction of Ago2 binding to multiple specific mitochondrial transcripts upon C2C12 differentiation (Figure 3C).

A major technical concern is potential contamination of abundant mitochondrial transcripts during immunoprecipitation, which might be the reason that most published CLIP-seq studies ignored tags that were mapped to mitochondrial transcripts. To address this problem, we analyzed crosslink-induced mutation sites (CIMS), which is known to occur in internal regions, while insertions and point mutations due to sequencing errors are typically distributed at both ends (Zhang and Darnell, 2011) (Figure S3D). The CIMSs (blue tags on the opposite side of red CLIP tags) were largely concordant with the distribution of the CLIP tags mapped on mitochondrial transcripts, thus confirming direct interactions (Figure 3C).

Importantly, using the PITA program, we identified potential target regions for the two most highly induced miR-1 (green bars) and miR-206 (red bars), which shared related seed sequences. Two of these predicated sites exactly match the miRACE-identified target sites for miR-1 in ND1 and COX1 (blue bars in Figure 3C). These candidate miR-1 target sites correspond to multiple induced Ago2 CLIP-seq peaks. Specifically, we noted a major Ago2 CLIP-seq peak on ND1 (peak 1), another major peak on ATP8 (peak 3), multiple peaks on COX3 (peak 4), two small peaks on ND5 (peak 5 and 6), and one peak on cytb (peak 7) (Figure 3C). Interestingly, Ago2 seems to prevalently interact with 12S mitochondria-specific rRNA (Rrn1) in myoblasts, which was further induced after C2C12 differentiation to myotubes. Furthermore, Ago2 also shows broad interactions with multiple mitochondrial transcripts, including COX1, which contains a miR-1 target that had been both predicted and experimentally mapped. This broad binding pattern implies either multiple miRNA:mRNA interactions and/or some distinct functional properties of Ago2 in the mitochondria (see Discussion).

Polysome Profiling of Mitochondrial Translation during Muscle Differentiation

A gold standard for studying translational control is through polysome profiling, a routine for investigating cytoplasmic translation, but a major challenge for detecting potential polysomes from the mitochondria partly because of coupled transcription/translation on the inner membrane (Bestwick and Shadel, 2013; Bonawitz et al., 2006). By optimizing the protocol for mitoribosome fractionation, we detected both small (28S) and large (39S) ribosome fractions as well as monosomes (55S) on a 10%–30% sucrose gradient, which is characterized by the distribution of 12S and 16S rRNAs and their associated ribosome proteins (MRPS27 and MRPL24) (Figure 3D). These profiles resemble closely to those reported in the literature (Antonicka et al., 2013; Surovtseva et al., 2011). Interestingly, we also detected putative polysomes near the bottom of the gradient (fractions 12 and 13) on both C2C12 myoblasts and myotubes, which could be converted to monosomes by RNase I treatment (Figure 3D).

Importantly, we observed that Ago2 cosediments with 28S and 39S ribosomes, and to a less extent, with monosomes or potential polysomes on myoblasts, and such distribution became broadened on myotubes, indicative of additional induced interactions (Figure 3D). This is consistent with Ago2 CLIP-seq signals on 12S rRNA in myoblasts and, to a less extent, 16S rRNA in myotubes (see Figure 3C). Significantly, by RT-qPCR quantification of ND1 and COX1 mRNAs and plotting the data according to percent distribution on the gradient, we found that both mitochondrial transcripts showed increased association with the putative polysome fractions from myotubes relative to myoblasts. These data provide initial support to enhanced mitochondrial translation upon C2C12 cell differentiation.

Opposite Functions of miR-1 in the Cytoplasm versus Mitochondria

To determine the precise role of miR-1 in mitochondrial translation, we first validated the expected effect of miR-1 on repressing translation of its cytoplasmic target HDAC4 (Chen et al., 2006) and the newly identified target ELL2 (Figure 4A). Interestingly, we detected the opposite effects of miR-1 on mitochondrial ND1 and COX1 transcripts in undifferentiated C2C12 cells, which showed increased, rather than decreased, translation, while the level of COX2 was unaffected (Figure 4B). Using Ago2 knockout mouse embryonic fibroblasts (MEFs), we demonstrated that the miR-1 effects on both COX1 and ND1 were Ago2-dependent (Figure 4C).

To further characterize this positive effect, we performed a converse experiment using an antagomir to block miR-1 in C2C12 myotubes (Figure 4D). While antagomir-1 had little effect on ND1 and COX1 proteins before miR-1 induction in C2C12 myoblasts, the miR-1 inhibitor diminished miR-1 expression detected by Northern and blocked enhanced ND1 and COX1 translation measured by western blotting (Figure 4D). Consistent with the regulation at the translational level, little difference was detected on the mRNA level for both of these mitochondrial transcripts (Figure 4D, bottom). We could also prevent miR-1-dependent translational enhancement by coexpressing a miR-1 sponge in the cytoplasm (Figure S4A).

As expected, the activities of ND1-containing Complex I and COX1-containing Complex IV were both elevated in miR-1 transfected myoblasts (Figure 4E). ATP production was also enhanced upon C2C12 differentiation, which was significantly attenuated by antagomir-1 (Figure 4F). Despite relatively modest enhancement in these assays, which might be due to uncoordinated induction of other respiratory chain components in miR-1 transfected cells, these results linked miR-1 enhanced translation to increased respiratory activities.

Base-Pairing Requirement for miR-1-Induced Mitochondrial Translation

To understand how miR-1 enhances mitochondrial translation, we first asked if there is anything unusual about the miR-1

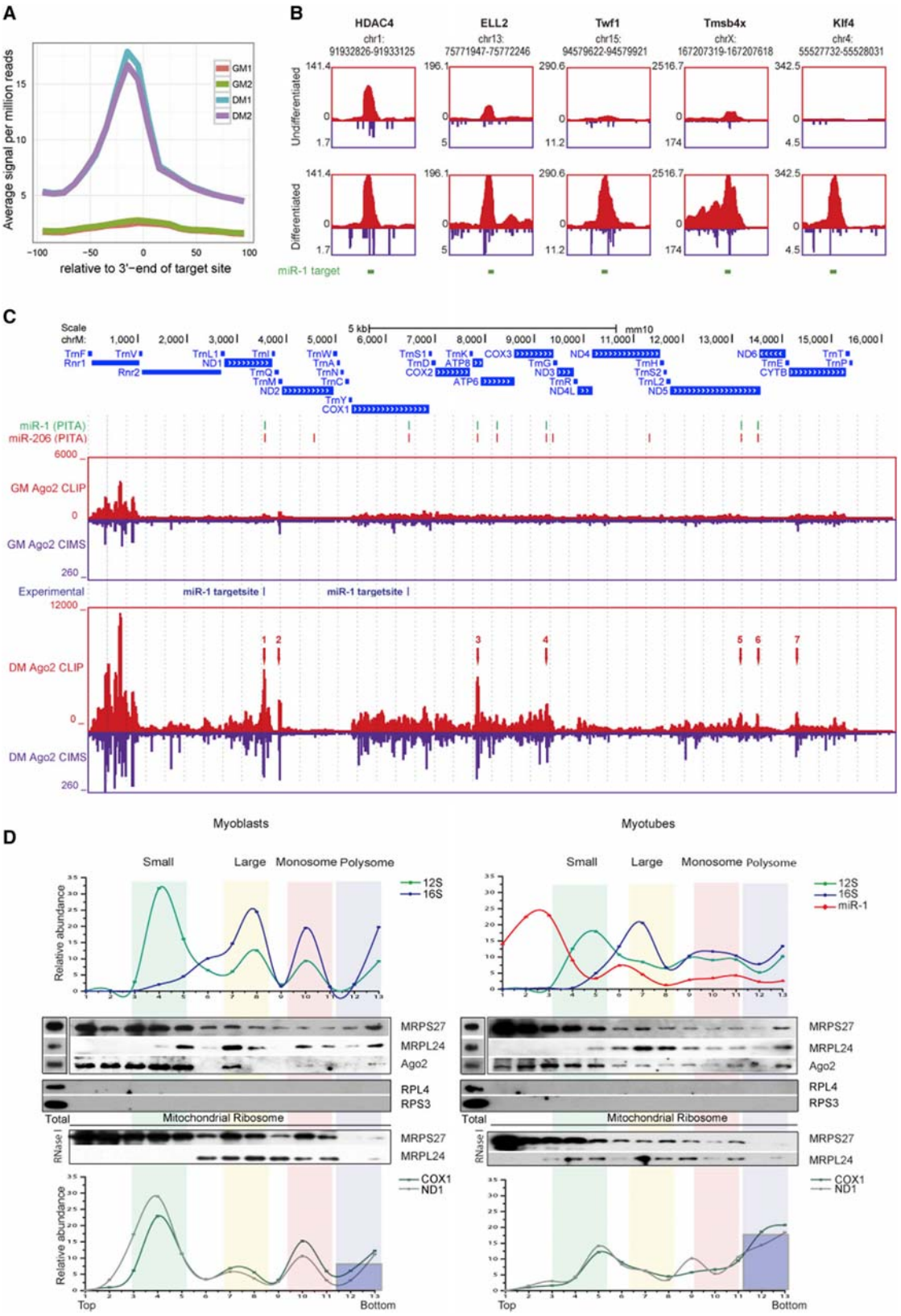

(legend on next page)

targeting site in ND1 or COX1. We found that, as expected, the target sites cloned in the 3′ UTR of a luciferase reporter mediated translational repression in the cytoplasm, and a mutant miR-1 lost the effect, which could be reversed by reverting the target sequences in the reporter to restore base pairing (Figures S4B and S4C). The stimulating effect of miR-1 did not seem to result from induced myogenesis or increased mtDNA replication (Figures S4D–S4F). We also found that miR-1 was able to enhance ND1 translation (Figure 4G) and ATP production (Figure 4H) in nonmyogenic HeLa cells. These data argue against enhanced mitochondrial translation as an indirect result of the induced myogenic program.

The mapped miR-1 target sites in both ND1 and COX1 fulfill the established base-pairing rule for miRNA targeting (Figure 5A). The seed regions in both COX1 and ND1 appear to be more conserved during evolution compared to those in the middle and the 3′ side (Figure S5A). We mutated either the seed region or the 3′ sequence and found that both mutations abolished miR-1-induced ND1 and COX1 translation (Figures 5A and 5B). Again, the mRNA levels remained unaltered, and neither wild-type miR-1 nor its mutants exhibited detectable effect on the nuclear DNA-encoded mitochondrial protein COX4 (Figure 5B).

Direct Action of miR-1 in Mitochondrial Translation

We took two additional strategies to further demonstrate the direct act of miR-1 within the mitochondria. We designed two separate miRNA mimics with altered targeting specificities. miR-COX1 would more efficiently target COX1, with reduced potential in targeting ND1, while miR-ND1 would only target ND1 (Figure 5C). The specificity of these designer miRNA mimics was confirmed on their cytoplasmic reporters (Figures S5B and S5C). In transfected C2C12 myoblasts, we found that miR-COX1 elevated COX1, with less effect on ND1, and as expected, miR-ND1 only stimulated ND1 (Figure 5D). We also tested another miRNA miR-101, which targets a specific region in ND1, and miR-499-5p, which targets a different region in ND1 (Figure 5E). We found that both exclusively enhanced ND1 translation, while several nontargeting miRNAs tested lacked the effect (Figure 5F). Because it is unlikely that specific miRNA mimics all caused the same indirect effects in the cytoplasm to stimulate mitochondrial translation, these data support the direct act of multiple miRNAs in enhancing mitochondrial translation.

To provide decisive evidence, we took advantage of Ago2 knockout MEFs to functionally rescue miR-1-dependent mitochondrial translation with either HA-tagged Ago2 or mitochondria-targeted Ago2 that carries a specific mitochondrial targeting signal peptide (su9). Confocal microscopy confirmed the colocalization of Su9-HA-Ago2 with Mito-GFP, a well-established marker for the mitochondria (Chen et al., 2003), while HA-Ago2 was diffusely localized in the cytoplasm (Figure 5G). Using an RNAi-based luciferase reporter containing a perfect complementary sequence to miR-1, we found that the reporter was potently suppressed in wild-type, but not in Ago2 knockout MEFs (Figure 5H, top). Exogenous HA-Ago2 rescued the RNAi effect and restored miR-1-enhanced translation of ND1 and COX1, and in sharp contrast, mitochondria-targeted Su9-HA-Ago2 could not rescue the RNAi effect in the cytoplasm, but potently restored the effect of miR-1 in the mitochondria (Figure 5H). Together with the specificity switch experiments, these data demonstrate the direct effect of miR-1 in enhancing mitochondrial translation.

Differential Sensitivity to Cytoplasmic and Mitochondrial Translational Inhibitors

Thus far, we had measured the steady state levels of mitochondrial proteins to infer miR-1 regulated translation. To directly demonstrate enhanced mitochondrial translation, we used the methionine analog AHA to metabolically label nascent proteins in the mitochondria while blocking cytoplasmic translation by Emetine (Weraarpachai et al., 2009). In this experimental setting, C2C12 myoblasts were first transfected with miR-1 and then switched to the media containing Emetine. AHA was next added to allow its incorporation into nascent polypeptides, which were subsequently labeled by the reaction with fluorescent alkyne and resolved on SDS-PAGE. As expected, Emetine plus the mitochondrial translation inhibitor Chloramphenicol (INN) potently blocked all translation activities in the cell (Figure 6A, lanes 3 and 4).

In the presence of Emetine, but absence of INN, we detected translation products of all mtDNA-encoded transcripts. Compared to loading controls, we noted some general enhancement

Figure 3. Mapping of Ago2-RNA Interactions by CLIP-Seq and Analysis of Mitochondrial Translation by Polysome Profiling

(A) Ago2 CLIP-seq profiles on predicted miR-1 targets before and after C2C12 differentiation. Duplicated data in each cell type were individually plotted against the center of PITA predicted miR-1 target sites.

(B) Ago2 CLIP tags on known cytoplasmic targets for miR-1 before (top) and after (bottom) C2C12 differentiation. The chromosomal location of each target site is shown on the top of each panel. Red, CLIP tags; blue, CIMS tags.

(C) The distribution of Ago2 CLIP-seq tags in the mitochondrial genome before and after C2C12 cell differentiation. The annotated genes are displayed on the top. PITA predicted target sites for miR-1 (green) and miR-206 (red) are indicated right below the gene track. The CLIP tag distribution (red) and corresponding CIMS (dark blue) are separately mapped to the mitochondrial genome in C2C12 myoblasts cultured in growth media (GM) and in C2C12 myotubes maintained in differentiation media (DM) for 4 days. The locations of miRACE identified miR-1 target sites are indicated between the two CLIP panels.

(D) Analysis of mitochondrial translation by polysome profiling. Purified mitochondria were used for fractionation on a sucrose gradient, which was free of cytoplasmic ribosomes, as indicated by the lack of western blotting for representative cytoplasmic ribosomal proteins (RPS3 and RPL4). Representative mitochondrial ribosomal proteins (MRPS27 and MRPL24) and Ago2 on individual gradient fractions were detected by western blotting and specific rRNA, mRNA, and miRNA transcripts were quantified by real-time RT-PCR (TaqMan for miR-1). The assignment of small and large ribosomal subunits, monosomes, and putative polysomes was based on the distribution of both rRNAs and proteins and comparison with published mitochondrial polysome profiles. The putative polysome fractions were characterized by RNase I treatment. The relative abundance of individual transcripts in each fraction was presented as the percentage of the total fraction. The increased polysome association of ND1 and COX1 transcripts is highlighted with dark blue bars proportional to their enhancement from myoblasts to myotubes.

See also Figure S3.

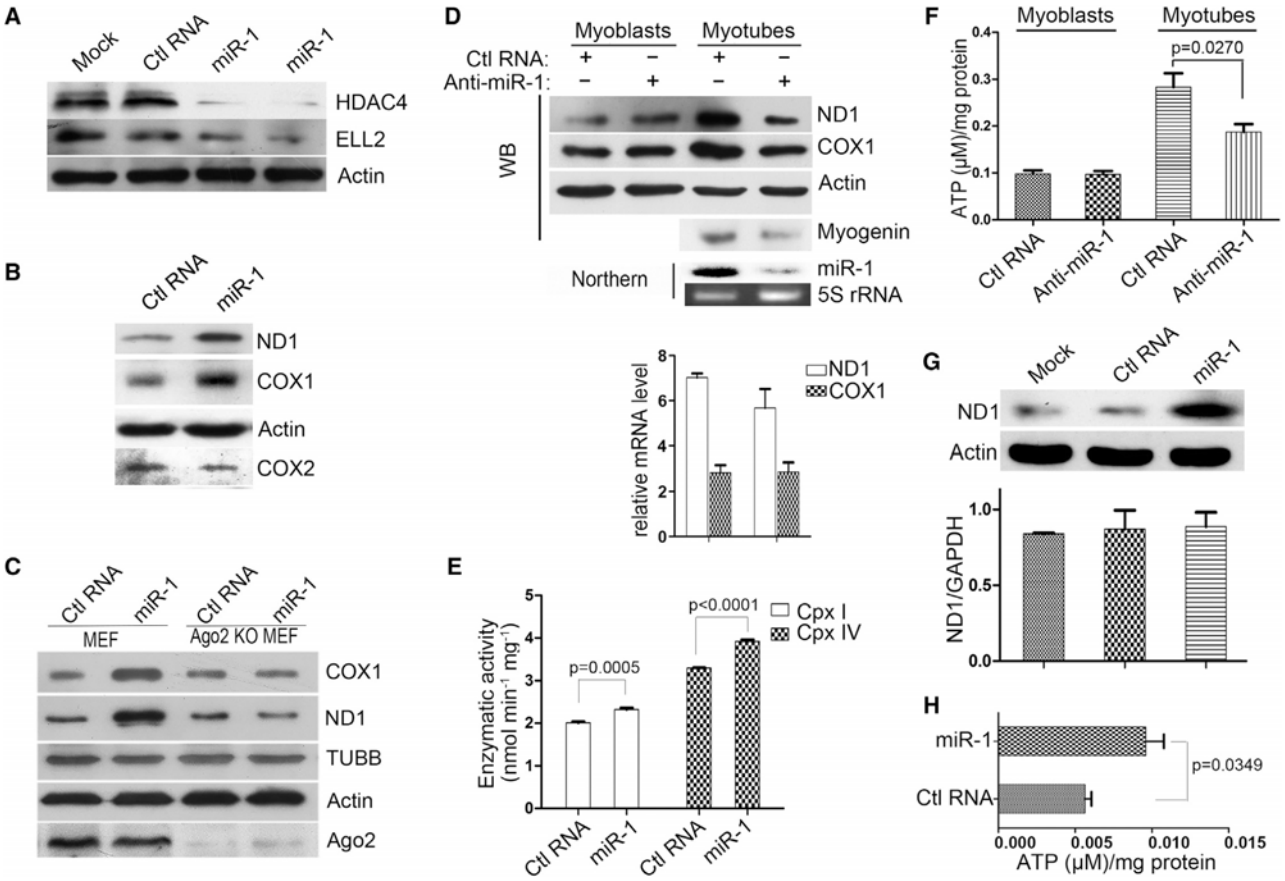

Figure 4. Opposite Effects of miRNAs on Translation in the Cytoplasm versus Mitochondria

(A) Western blotting of HDAC4 and ELL2 in C2C12 myoblasts after transfection with miR-1 or control siRNA.

(B) Western blotting of ND1 and COX1 in C2C12 myoblasts 48 hr after transfection with control RNA or miR-1.

(C) ND1 and COX1 protein levels in wild-type and Ago2 knockout MEFs transfected with either control RNA or miR-1.

(D) Antagomir-1 blocked miR-1 expression and diminished enhanced ND1 and COX1 translation in myotubes. In this experiment, C2C12 myoblasts were first transfected with control RNA or antagomir-1 and subsequently transferred to differentiation media after 24 hr. Western blotting of ND1 and COX1 was performed after culturing the cells for another 3 days. Actin and 5S rRNA served as loading controls for protein and RNA. The lower panel showed that antagomir-1 had no effect on the mRNA levels of both ND1 and COX1.

(E) Enhanced activities of Complex I and IV by miR-1 in transfected C2C12 myoblasts.

(F) Antagomir-1 blocked enhanced ATP production in C2C12 myotubes.

(G) miR-1 enhanced ND1 protein synthesis without affecting its mRNA levels in transfected HeLa cells.

(H) miR-1 induced ATP production in transfected HeLa cells.

Data in (D–H) are based on three biological repeats and shown as mean ± SD; p values are indicated in each panel. Specific microRNA mimics and antagomirs are listed in Table S3. See also Figure S4.

of mitochondrial translation by miR-1. In addition, miR-1 markedly enhanced COX1 translation (Figure 6A, compare lanes 5 and 6). We also reproducibly detected enhanced (although to less degrees) translation of ND1 (note that ND1 was less efficiently labeled, which is a well-known fact) as well as cytb, COX3, and ATP8 (red arrows in Figure 6A), all of which contain at least one predicted miR-1 targeting site each underlying a specific Ago2 CLIP-seq peak (see Figure 3C). In contrast, overexpressed miR-499-5p had no effect on COX1, but enhanced ND1 translation (Figure 6A, lanes 7 and 8), consistent with its targeting specificity. We also noted its ability to enhance ND4L translation, which also contains a predicted miR-499-5p targeting site (data not shown). Finally, using INN, we examined and ruled out the potential effect of miR-1 on the protein stability of ND1 (Figure 6B). Together, these data provide concrete evidence for miRNA-augmented mitochondrial translation.

Potential Mechanism for miRNA-Enhanced Translation in the Mitochondria

To gain mechanistic insights into miRNA-enhanced mitochondrial translation, we followed the clue from a *Drosophila* study, which suggests three critical requirement for converting miRNA-dependent translational repression to activation: (1) lack of the cap at the 5′ end, (2) lack of a typical poly(A) tail at the 3′ end, and (3) detachment of GW182 from an Ago protein (Iwasaki and Tomari, 2009; Vasudevan, 2012). Interestingly, all

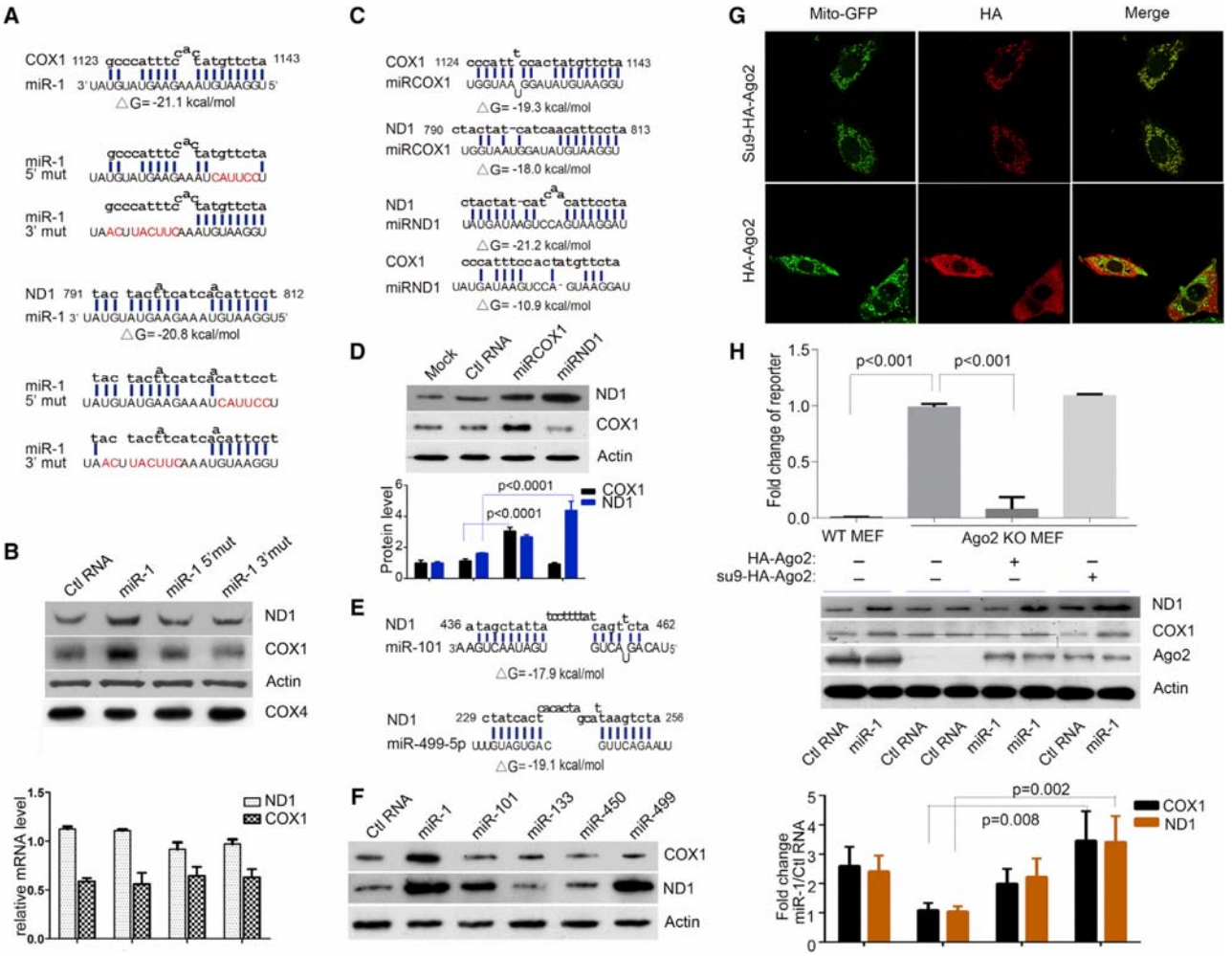

Figure 5. Target-Specific Effect of miRNA and miRNA Mimics

(A) Sequences of miR-1 and its 3′ and 5′ mutants. Calculated free energy for base-pairing is indicated for wild-type miR-1.

(B) Analysis of C2C12 myoblasts transfected with wild-type and mutant miR-1 by western blotting (top) and real-time RT-qPCR (bottom). Data in the bottom panel are based on triplicated experiments and shown as mean ± SD.

(C) Designer miRNA mimics and their base-pairing potential with COX1 and ND1. According to the calculated free energy, miRCOX1 showed reduced base pairing with ND1 whereas miRND1 lost the ability to base pair with COX1.

(D) Analysis of C2C12 myoblasts transfected with miRCOX1 and miRND1 by western (top) and specific proteins levels were quantified (bottom). Data are based on triplicated experiments and error bars are means ± SD.

(E) Base-pairing potentials of a miR-101 and miR-499-5p with distinct regions in the ND1 transcript.

(F) Analysis of C2C12 myoblasts transfected with a panel of miRNAs, two of which (miR-101 and miR-499-5p) enhanced ND1, but not COX1, protein synthesis. miR-1 effects were analyzed in parallel as a positive control. See also Figure S5.

(G) Confocal microscopic analysis of Ago2 knockout MEFs complemented with HA-Ago2 or mitochondrial targeted Su9-HA-Ago2. Mitochondria was marked by a cotransfected Mito-GFP.

(H) General and selective rescue of Ago2 functions on Ago2 knockout MEFs. A luciferase reporter containing a perfectly complementary sequence to miR-1 was analyzed to determine the Ago2-mediated RNAi effect in the cytoplasm (top). The data showed that the RNAi effect could be rescued by HA-Ago2, but not mitochondria- targeted Su9-HA-Ago2. The expression of tagged Ago2 and the response of ND1 and COX1 translation to transfected miR-1 in different Ago2 complemented MEFs were shown in the middle. The data of triplicated experiments were quantified and shown as mean ± SD with indicated p values (bottom). Specific microRNA mimics are listed in Table S3.

mitochondrial transcripts automatically fulfill the first two requirements because mitochondrial transcripts resemble mRNAs in prokaryotic cells by having no cap nor typical long poly(A) tail (Gagliardi et al., 2004; Temperley et al., 2010). This prompted us to experimentally test the third requirement by determining whether GW182 maintains its partnership with Ago2 within the mitochondria.

We found that, compared to Ago2, GW182 was only detected in the cytoplasm (Figure 6C). Three GW182 paralogs are encoded in mammalian genomes, including TNRC6A (that

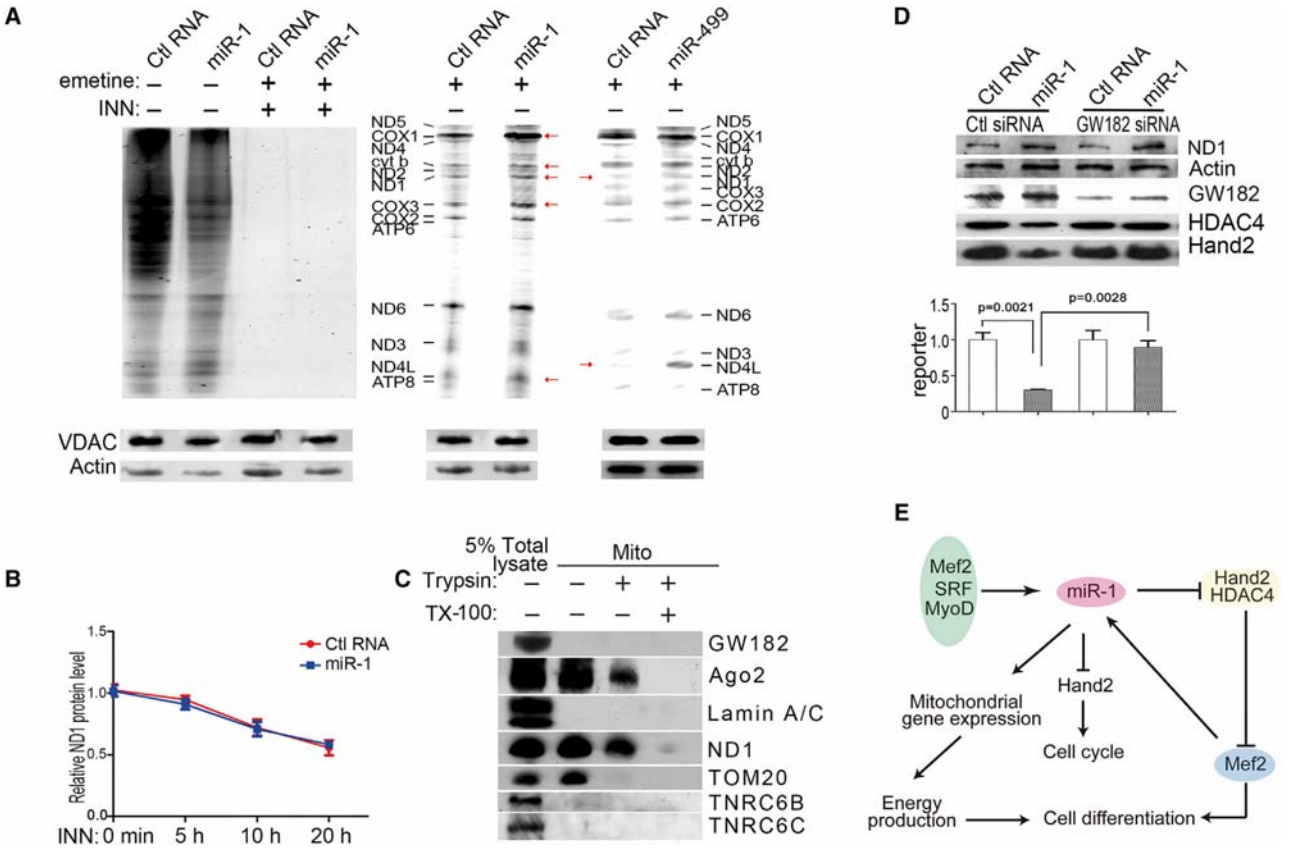

Figure 6. miR-1 Enhanced Protein Synthesis in the Mitochondria

(A) Detection of nascent protein synthesis in the mitochondria when cytoplasmic translation was blocked by Emetine. C2C12 myoblasts were first transfected with a control RNA or miR-1 or miR-499-5p and protein synthesis was monitored by AHA incorporation in the presence of Emetine. Cytoplasmic actin and mitochondrial VDAC served as loading controls. Emetine blocked all cytoplasmic translation to allow detection of mitochondrial translational activities. Red arrows highlight individual elevated bands by miR-1 or miR-499-5p.

(B) Lack of effect of miR-1 on ND1 protein stability. The protein levels were determined in the presence of INN in control and miR-1 transfected C2C12 cells and the data were normalized against the protein level of ND1 at the 0 time point.

(C) Restriction of GW182 and its paralogs TNRC6B and TNRC6C from the mitochondria. Lamin A/C was purified away from the mitochondria. ND1 and Tom20 served as controls for proteins localized within the mitochondria or associated with the outer membrane of purified mitochondria.

(D) miR-1 enhanced mitochondrial translation when the miRNA machinery was selectively inactivated by knocking down GW182 in the cytoplasm. GW182 showed the expected requirement for miR-1 to act on its cytoplasmic targets HDAC4 and Hand2 (top) and on a cytoplasmic luciferase reporter containing the miR-1 targeting site in ND1 (bottom). When the function of the miRNA machinery was largely compromised in the cytoplasm of GW182 knockdown cells (using specific siRNAs listed in Table S3), transfected miR-1 continued to show the ability to enhance ND1 translation in the mitochondria.

(E) Expanded roles of miR-1 in muscle differentiation. miR-1 is known to be induced by SRF, MyoD and Mef2 during differentiation. Induced miR-1 has been thought to act on its cytoplasmic targets to inhibit cell proliferation via Hand2 and promote cell differentiation through HDAC4 and Mef2. The newly elucidated function of miR-1 contributes to efficient protein synthesis in the mitochondria, resulting in boosted ATP production to meet the increasing energy demand in differentiating muscle cells. Therefore, miR-1 mediated translational repression in the cytoplasm and translational enhancement in the mitochondria may constitute a highly coordinated myogenic program for muscle differentiation and function.

Data in (B) and (D) are based on three biological repeats and shown as mean ± SD with p values indicated in (D).

corresponds to GW182), TNRC6B and TNRC6C (Ding and Han, 2007; Jakymiw et al., 2007) and published works indicate that all function in the miRNA pathway (Liu et al., 2005; Meister et al., 2005; Zipprich et al., 2009). We found that all three GW182 family members were excluded from the mitochondria (Figure 6C), suggesting that the miRNA machinery is rearranged in the mitochondria.

We took advantage of this mechanistic insight to further test the selective requirement for GW182 in miRNA-mediated functions in the cytoplasm versus the mitochondria. GW182 has been shown to be required for miRNA-mediated translational repression in the cytoplasm (Eulalio et al., 2008; Zipprich et al., 2009). As expected, GW182 knockdown prevented miR-1-mediated translational repression of its two cytoplasmic targets HDAC4 and Hand2 (Figure 6D, top) as well as the cytoplasmic reporter containing the miRNA target site from ND1 (Figure 6D, bottom). Under these conditions, GW182 RNAi-treated C2C12 myoblasts continued to show enhanced ND1 translation by miR-1 (Figure 6D, top). Based on these results, we propose that the rearranged miRNA machinery, coupled with the

prokaryotic characteristics of the mitochondrial transcripts, is responsible for translational enhancement in the mitochondria.

DISCUSSION

The findings presented in this article have important implications in diverse functions of the miRNA machinery in mammalian cells, miRNA-mediated switch of energy sources during cellular differentiation and reprogramming, and initiation of mitochondrial translation, which has been poorly understood despite intensive efforts in past decades. Below we discuss critical insights into each of these functional aspects.

Selective Targeting of Ago2 and Specific miRNAs to the Mitochondria

The presence of the miRNA machinery in the mitochondria was only recently recognized (Bandiera et al., 2011; Barrey et al., 2011; Bian et al., 2010; Das et al., 2012; Kren et al., 2009; Sripada et al., 2012). In the present study, we carefully examined this critical issue by using highly purified mitoplasts to perform protease and nuclease protection assays and employed quantitative data to demonstrate that a significant fraction of Ago2 and miR-1 indeed reside within the mitochondria, especially when C2C12 cells are differentiated into myotubes.

An important question is how Ago2 is able to selectively enter the mitochondria. A previous study predicted a mitochondrial targeting sequence near the N terminus of the Ago2 protein (Bandiera et al., 2011). We fused this sequence to GFP, but failed to detect its ability to target GFP to the mitochondria (data not shown). While still a mystery, it is important to note that most nuclear DNA-encoded mitochondrial proteins do not contain any identifiable mitochondrial targeting sequences, indicating the existence of other mechanisms for importing cytoplasmic proteins into the mitochondria, such as communication between mitochondria and ER where Ago2 was initially identified (Cikaluk et al., 1999; Kornmann et al., 2009).

Although 5S rRNA and tRNA can be actively imported into mitochondria (Mahata et al., 2006; Wang et al., 2010), we do not know how exactly miRNAs enter the mitochondria. Our preliminary mitochondrial import assay indicates that multiple specific and nonspecific miRNAs, but not their precursors, were able to enter purified mitochondria without the need for ATP hydrolysis (data not shown). We thus suspect that, while most miRNAs may be tied up on their cytoplasmic targets, thus preventing them from free diffusion, a subset of "free" miRNAs, including those newly induced, might enter the mitochondria. Clearly, the mechanism for targeting a subset of miRNAs and specific components of the miRNA machinery to the mitochondria awaits future studies.

Enhanced Translation by the miRNA/Ago2 Complex in the Mitochondria

We provided a series of evidence for direct action of the miRNA/Ago2 complex in enhancing mitochondrial translation, including (1) direct Ago2 binding to specific mtDNA-encoded transcripts, (2) the requirement for specific base-pairing interactions to elicit the effect, (3) functional rescue of Ago2 knockout MEFs with mitochondria-targeted Ago2, and (4) selective inactivation of the miRNA machinery in the cytoplasm by GW182 knockdown. The latter two pieces of information demonstrate that miR-1 is able to stimulate mitochondrial translation when the miRNA machinery is selectively inactivated in the cytoplasm.

It is currently unclear how the miRNA/Ago2 complex precisely augments mitochondrial translation. In fact, this is related to a fundamental question with respect to translation initiation in the mitochondria, despite of extensive efforts in the past decades. This is because the fully processed mitochondrial transcripts do not contain a cap structure (a key feature of eukaryotic cytoplasmic mRNAs) nor contain any identifiable ribosomal binding site (a mechanism used by bacteria). Based on our Ago2 mapping data, it is curious to note extensive interactions of Ago2 with the 12S rRNA. We also observed extensive association of Ago2 with mitochondrial transcripts, some with more specific interactions while others in a more continuous fashion as if those transcripts are "wrapped" around the Ago2-containing complex. As such, Ago2 may function as a key mitochondrial translation initiation factor to facilitate ribosome-mRNA interactions.

A Coordinated Myogenic Program Regulated by miR-1

Our findings also extend the physiological function of miR-1 in skeletal and cardiac muscle. Genetic ablation of this miRNA demonstrated a profound effect on heart functions in the mouse (Zhao et al., 2007). However, as the heart contains fully differentiated cardiomyocytes in adult, it has been unclear how this miRNA might contribute to muscle physiology. Our data demonstrate that this miRNA is able to boost ATP production in the mitochondria, which is in high demand for heart contraction, thus providing a plausible explanation for its functional requirement in the heart.

Published studies have demonstrated a vital role of miR-1 in inhibiting HDAC4 (Chen et al., 2006), which suppresses Mef2 (Arnold et al., 2007), and elevated Mef2 further activates the expression of miR-1 (Liu et al., 2007), thereby forming an autoregulatory loop to maintain the myogenic program. Our data add a further role of miR-1 in enhancing protein synthesis and ATP production in the mitochondria of differentiated muscle cells and suggest miR-1 in coordinating regulatory networks in both the cytoplasm and the mitochondria during and after muscle differentiation, as illustrated in Figure 6E. Therefore, the newly elucidated role of the miRNA complex in the mitochondria suggests a new layer of crosstalk between nuclear and mitochondrial genomes in eukaryotic cells.

EXPERIMENTAL PROCEDURES

Isolation of Mitochondria and Purification of Mitoplasts

Cardiomyocytes from mouse heart, C2C12-derived myoblasts or myotubes were collected by centrifugation, homogenized in a prechilled Dounce homogenizer (Kontes), and postnuclear supernatant collected. Mitochondria were sedimented at 13,000 × *g* for 10 min, washed once in the same buffer, and further purified by centrifugation at 40,000 × *g* for 1 hr at 4°C on a sucrose gradient (17%, 31%, 42%, 50%) in $T_{10}E_{20}$ buffer (10 mM Tris-HCl pH 7.4, 20 mM EDTA). Purification of mitoplasts was according to the previous procedure (Schnaitman and Greenawalt, 1968). Table S3 lists specific microRNA mimics and antagomirs tested on mitochondrial transcripts.

Trypsin/Nuclease Protection Assays

For trypsin protection, isolated mitochondria and mitoplasts were either kept on ice as control or treated with Trypsin (100 μg/ml) alone or with Trypsin (100 μg/ml) plus Triton X-100 (1%). Treated mitochondria or mitoplasts were collected by centrifugation at 18,000 × *g* for 3 min and the pellets were resuspended in SDS-PAGE sample buffer for western blotting. The nuclease protection was similarly performed on isolated mitochondria and mitoplasts with RNase T1 (3,000 U/ml) plus Micrococcal nuclease (1,000 U/ml) digestion on ice for 30 min in the presence or absence of Triton X-100. RNA was extracted with Trizol from pelleted mitochondria or mitoplasts for RT-qPCR. PCR primers and probes are listed in Table S4.

Analysis of Mitochondrial Translation by Polysome Profiling

Sucrose gradient sedimentation of mitochondrial ribosome/polysome was carried out as described (Antonicka et al., 2013). Briefly, mitochondria purified from C2C12 myoblasts or myotubes were suspended in the lysis buffer (260 mM sucrose, 100 mM KCl, 20 mM $MgCl_2$, 10 mM Tris-pH 7.5, 1% Triton X-100, 5 mM β-mercaptoethanol, and a cocktail of protease inhibitors from Roche) on ice for 20 min. The lysate was centrifuged at 9,000 × *g* for 30 min to remove particles, loaded on an 8 ml 10%–30% sucrose gradient, and centrifuged at 180,000 × *g* for 260 min in a Beckman SW41-Ti rotor. To characterize putative polysomes, the lysate was treated with 5 U/μl RNase I for 40 min at 25°C. After centrifugation, 13 fractions were collected for RNA and protein analysis.

Detection of Nascent Protein Synthesis

Click-iT reagents (Life Technology) were used to label nascent polypeptides. C2C12 myoblasts were first transfected with miRNA or control RNA at 30%–40% confluence in 24-well plates. After culturing overnight, the plate was washed three times with prewarmed PBS. The cells were incubated in methionine-free DMEM for 45 min followed by the addition of 20 μM of Emetine, and incubated for another 15 min. The media were replaced with methionine-free DMEM containing 50 μM methionine analog AHA and 20 μM Emetine. After incubation for 4 hr, AHA-containing nascent proteins were labeled with TAMRA (Life Technology), resolved in 4%–12% gradient SDS-PAGE, and analyzed by Typhoon 9400. These and other methods are detailed in Extended Experimental Procedures.

ACCESSION NUMBERS

The Gene Expression Omnibus accession number for the Ago2 CLIP-seq data performed on C2C12 myoblasts and myotubes reported in this paper is GSE57596.

SUPPLEMENTAL INFORMATION

Supplemental Information includes Extended Experimental Procedures, five figures, and four tables and can be found with this article online at http://dx.doi.org/10.1016/j.cell.2014.05.047.

AUTHOR CONTRIBUTIONS

X-R.Z., X-X.Z., and X-D.F. designed the experiments. Y.Z. contributed to experimental design in the initial phase of this project. X-R.Z., X-X.Z., and L.Z. carried out most of the experiments. Y.X. performed Ago2 CLIP-seq. B.Y., Y.Z., J.H., J.Z., and Y.Y. analyzed the data. X-L.Z. and L.G. performed mass spectromic analysis of IPed Ago2. H.Z., P.G., and H.S. contributed to data collection. X-R.Z., X-X.Z., and X-D.F. wrote the paper.

ACKNOWLEDGMENTS

We thank Drs. Immo Scheffler, Amy Pasquinelli, Shobha Vasudevan, and David Chan for insightful discussion during the course of this investigation, Dr. Xiaoyan Ding for providing the C2C12 cell line, and Dr. Anna Lombes for the gift of anti-ND1 antibody. This work was supported by the China 973 program (2011CB811300, 2012CB910800), the Chinese 111 program grant (B06018), and NIH grants (GM049369 and GM052872).

Received: September 18, 2013
Revised: April 15, 2014
Accepted: May 29, 2014
Published: July 31, 2014

REFERENCES

Antonicka, H., Sasarman, F., Nishimura, T., Paupe, V., and Shoubridge, E.A. (2013). The mitochondrial RNA-binding protein GRSF1 localizes to RNA granules and is required for posttranscriptional mitochondrial gene expression. Cell Metab. *17*, 386–398.

Arnold, M.A., Kim, Y., Czubryt, M.P., Phan, D., McAnally, J., Qi, X., Shelton, J.M., Richardson, J.A., Bassel-Duby, R., and Olson, E.N. (2007). MEF2C transcription factor controls chondrocyte hypertrophy and bone development. Dev. Cell *12*, 377–389.

Bandiera, S., Rüberg, S., Girard, M., Cagnard, N., Hanein, S., Chrétien, D., Munnich, A., Lyonnet, S., and Henrion-Caude, A. (2011). Nuclear outsourcing of RNA interference components to human mitochondria. PLoS ONE *6*, e20746.

Barrey, E., Saint-Auret, G., Bonnamy, B., Damas, D., Boyer, O., and Gidrol, X. (2011). Pre-microRNA and mature microRNA in human mitochondria. PLoS ONE *6*, e20220.

Bestwick, M.L., and Shadel, G.S. (2013). Accessorizing the human mitochondrial transcription machinery. Trends Biochem. Sci. *38*, 283–291.

Bian, Z., Li, L.M., Tang, R., Hou, D.X., Chen, X., Zhang, C.Y., and Zen, K. (2010). Identification of mouse liver mitochondria-associated miRNAs and their potential biological functions. Cell Res. *20*, 1076–1078.

Bonawitz, N.D., Clayton, D.A., and Shadel, G.S. (2006). Initiation and beyond: multiple functions of the human mitochondrial transcription machinery. Mol. Cell *24*, 813–825.

Bosmann, H.B., Myers, M.W., Dehond, D., Ball, R., and Case, K.R. (1972). Mitochondrial autonomy. Sialic acid residues on the surface of isolated rat cerebral cortex and liver mitochondria. J. Cell Biol. *55*, 147–160.

Carthew, R.W., and Sontheimer, E.J. (2009). Origins and Mechanisms of miRNAs and siRNAs. Cell *136*, 642–655.

Cavelier, L., Johannisson, A., and Gyllensten, U. (2000). Analysis of mtDNA copy number and composition of single mitochondrial particles using flow cytometry and PCR. Exp. Cell Res. *259*, 79–85.

Cernilogar, F.M., Onorati, M.C., Kothe, G.O., Burroughs, A.M., Parsi, K.M., Breiling, A., Lo Sardo, F., Saxena, A., Miyoshi, K., Siomi, H., et al. (2011). Chromatin-associated RNA interference components contribute to transcriptional regulation in Drosophila. Nature *480*, 391–395.

Chekulaeva, M., and Filipowicz, W. (2009). Mechanisms of miRNA-mediated post-transcriptional regulation in animal cells. Curr. Opin. Cell Biol. *21*, 452–460.

Chen, H., Detmer, S.A., Ewald, A.J., Griffin, E.E., Fraser, S.E., and Chan, D.C. (2003). Mitofusins Mfn1 and Mfn2 coordinately regulate mitochondrial fusion and are essential for embryonic development. J. Cell Biol. *160*, 189–200.

Chen, J.F., Mandel, E.M., Thomson, J.M., Wu, Q., Callis, T.E., Hammond, S.M., Conlon, F.L., and Wang, D.Z. (2006). The role of microRNA-1 and microRNA-133 in skeletal muscle proliferation and differentiation. Nat. Genet. *38*, 228–233.

Cikaluk, D.E., Tahbaz, N., Hendricks, L.C., DiMattia, G.E., Hansen, D., Pilgrim, D., and Hobman, T.C. (1999). GERp95, a membrane-associated protein that belongs to a family of proteins involved in stem cell differentiation. Mol. Biol. Cell *10*, 3357–3372.

Czech, B., and Hannon, G.J. (2011). Small RNA sorting: matchmaking for Argonautes. Nat. Rev. Genet. *12*, 19–31.

Das, S., Ferlito, M., Kent, O.A., Fox-Talbot, K., Wang, R., Liu, D., Raghavachari, N., Yang, Y., Wheelan, S.J., Murphy, E., and Steenbergen, C. (2012).

Nuclear miRNA regulates the mitochondrial genome in the heart. Circ. Res. *110*, 1596–1603.

de Brito, O.M., and Scorrano, L. (2008). Mitofusin 2 tethers endoplasmic reticulum to mitochondria. Nature *456*, 605–610.

Ding, L., and Han, M. (2007). GW182 family proteins are crucial for microRNA-mediated gene silencing. Trends Cell Biol. *17*, 411–416.

Easow, G., Teleman, A.A., and Cohen, S.M. (2007). Isolation of microRNA targets by miRNP immunopurification. RNA *13*, 1198–1204.

Eulalio, A., Huntzinger, E., and Izaurralde, E. (2008). GW182 interaction with Argonaute is essential for miRNA-mediated translational repression and mRNA decay. Nat. Struct. Mol. Biol. *15*, 346–353.

Franko, A., Mayer, S., Thiel, G., Mercy, L., Arnould, T., Hornig-Do, H.T., Wiesner, R.J., and Goffart, S. (2008). CREB-1alpha is recruited to and mediates up-regulation of the cytochrome c promoter during enhanced mitochondrial biogenesis accompanying skeletal muscle differentiation. Mol. Cell. Biol. *28*, 2446–2459.

Gagliardi, D., Stepien, P.P., Temperley, R.J., Lightowlers, R.N., and Chrzanowska-Lightowlers, Z.M. (2004). Messenger RNA stability in mitochondria: different means to an end. Trends Genet. *20*, 260–267.

Guang, S., Bochner, A.F., Pavelec, D.M., Burkhart, K.B., Harding, S., Lachowiec, J., and Kennedy, S. (2008). An Argonaute transports siRNAs from the cytoplasm to the nucleus. Science *321*, 537–541.

Iwasaki, S., and Tomari, Y. (2009). Argonaute-mediated translational repression (and activation). Fly (Austin) *3*, 204–206.

Jakymiw, A., Pauley, K.M., Li, S., Ikeda, K., Lian, S., Eystathioy, T., Satoh, M., Fritzler, M.J., and Chan, E.K. (2007). The role of GW/P-bodies in RNA processing and silencing. J. Cell Sci. *120*, 1317–1323.

Kertesz, M., Iovino, N., Unnerstall, U., Gaul, U., and Segal, E. (2007). The role of site accessibility in microRNA target recognition. Nat. Genet. *39*, 1278–1284.

Kornmann, B., Currie, E., Collins, S.R., Schuldiner, M., Nunnari, J., Weissman, J.S., and Walter, P. (2009). An ER-mitochondria tethering complex revealed by a synthetic biology screen. Science *325*, 477–481.

Kren, B.T., Wong, P.Y., Sarver, A., Zhang, X., Zeng, Y., and Steer, C.J. (2009). MicroRNAs identified in highly purified liver-derived mitochondria may play a role in apoptosis. RNA Biol. *6*, 65–72.

Liu, J., Rivas, F.V., Wohlschlegel, J., Yates, J.R., 3rd, Parker, R., and Hannon, G.J. (2005). A role for the P-body component GW182 in microRNA function. Nat. Cell Biol. *7*, 1261–1266.

Liu, N., Williams, A.H., Kim, Y., McAnally, J., Bezprozvannaya, S., Sutherland, L.B., Richardson, J.A., Bassel-Duby, R., and Olson, E.N. (2007). An intragenic MEF2-dependent enhancer directs muscle-specific expression of microRNAs 1 and 133. Proc. Natl. Acad. Sci. USA *104*, 20844–20849.

Lopaschuk, G.D., Ussher, J.R., Folmes, C.D., Jaswal, J.S., and Stanley, W.C. (2010). Myocardial fatty acid metabolism in health and disease. Physiol. Rev. *90*, 207–258.

Mahata, B., Mukherjee, S., Mishra, S., Bandyopadhyay, A., and Adhya, S. (2006). Functional delivery of a cytosolic tRNA into mutant mitochondria of human cells. Science *314*, 471–474.

Meister, G., Landthaler, M., Peters, L., Chen, P.Y., Urlaub, H., Lührmann, R., and Tuschl, T. (2005). Identification of novel argonaute-associated proteins. Curr. Biol. *15*, 2149–2155.

Mortensen, R.D., Serra, M., Steitz, J.A., and Vasudevan, S. (2011). Posttranscriptional activation of gene expression in Xenopus laevis oocytes by microRNA-protein complexes (microRNPs). Proc. Natl. Acad. Sci. USA *108*, 8281–8286.

Moyes, C.D., Mathieu-Costello, O.A., Tsuchiya, N., Filburn, C., and Hansford, R.G. (1997). Mitochondrial biogenesis during cellular differentiation. Am. J. Physiol. *272*, C1345–C1351.

Rao, P.K., Kumar, R.M., Farkhondeh, M., Baskerville, S., and Lodish, H.F. (2006). Myogenic factors that regulate expression of muscle-specific microRNAs. Proc. Natl. Acad. Sci. USA *103*, 8721–8726.

Rizzuto, R., Pinton, P., Carrington, W., Fay, F.S., Fogarty, K.E., Lifshitz, L.M., Tuft, R.A., and Pozzan, T. (1998). Close contacts with the endoplasmic reticulum as determinants of mitochondrial Ca2+ responses. Science *280*, 1763–1766.

Saraste, M. (1999). Oxidative phosphorylation at the fin de siècle. Science *283*, 1488–1493.

Schnaitman, C., and Greenawalt, J.W. (1968). Enzymatic properties of the inner and outer membranes of rat liver mitochondria. J. Cell Biol. *38*, 158–175.

Sripada, L., Tomar, D., Prajapati, P., Singh, R., Singh, A.K., and Singh, R. (2012). Systematic analysis of small RNAs associated with human mitochondria by deep sequencing: detailed analysis of mitochondrial associated miRNA. PLoS ONE *7*, e44873.

Suh, N., Baehner, L., Moltzahn, F., Melton, C., Shenoy, A., Chen, J., and Blelloch, R. (2010). MicroRNA function is globally suppressed in mouse oocytes and early embryos. Curr. Biol. *20*, 271–277.

Surovtseva, Y.V., Shutt, T.E., Cotney, J., Cimen, H., Chen, S.Y., Koc, E.C., and Shadel, G.S. (2011). Mitochondrial ribosomal protein L12 selectively associates with human mitochondrial RNA polymerase to activate transcription. Proc. Natl. Acad. Sci. USA *108*, 17921–17926.

Taanman, J.W. (1999). The mitochondrial genome: structure, transcription, translation and replication. Biochim. Biophys. Acta *1410*, 103–123.

Temperley, R.J., Wydro, M., Lightowlers, R.N., and Chrzanowska-Lightowlers, Z.M. (2010). Human mitochondrial mRNAs—like members of all families, similar but different. Biochim. Biophys. Acta *1797*, 1081–1085.

Vasudevan, S. (2012). Posttranscriptional upregulation by microRNAs. Wiley Interdiscip Rev RNA *3*, 311–330.

Vasudevan, S., Tong, Y., and Steitz, J.A. (2007). Switching from repression to activation: microRNAs can up-regulate translation. Science *318*, 1931–1934.

Wang, G., Chen, H.W., Oktay, Y., Zhang, J., Allen, E.L., Smith, G.M., Fan, K.C., Hong, J.S., French, S.W., McCaffery, J.M., et al. (2010). PNPASE regulates RNA import into mitochondria. Cell *142*, 456–467.

Wang, D., Zhang, Z., O'Loughlin, E., Lee, T., Houel, S., O'Carroll, D., Tarakhovsky, A., Ahn, N.G., and Yi, R. (2012). Quantitative functions of Argonaute proteins in mammalian development. Genes Dev. *26*, 693–704.

Wei, W., Ba, Z., Gao, M., Wu, Y., Ma, Y., Amiard, S., White, C.I., Rendtlew Danielsen, J.M., Yang, Y.G., and Qi, Y. (2012). A role for small RNAs in DNA double-strand break repair. Cell *149*, 101–112.

Weraarpachai, W., Antonicka, H., Sasarman, F., Seeger, J., Schrank, B., Kolesar, J.E., Lochmüller, H., Chevrette, M., Kaufman, B.A., Horvath, R., and Shoubridge, E.A. (2009). Mutation in TACO1, encoding a translational activator of COX I, results in cytochrome c oxidase deficiency and late-onset Leigh syndrome. Nat. Genet. *41*, 833–837.

Zhang, C., and Darnell, R.B. (2011). Mapping in vivo protein-RNA interactions at single-nucleotide resolution from HITS-CLIP data. Nat. Biotechnol. *29*, 607–614.

Zhang, Y., Liu, D., Chen, X., Li, J., Li, L., Bian, Z., Sun, F., Lu, J., Yin, Y., Cai, X., et al. (2010). Secreted monocytic miR-150 enhances targeted endothelial cell migration. Mol. Cell *39*, 133–144.

Zhao, Y., Ransom, J.F., Li, A., Vedantham, V., von Drehle, M., Muth, A.N., Tsuchihashi, T., McManus, M.T., Schwartz, R.J., and Srivastava, D. (2007). Dysregulation of cardiogenesis, cardiac conduction, and cell cycle in mice lacking miRNA-1-2. Cell *129*, 303–317.

Zipprich, J.T., Bhattacharyya, S., Mathys, H., and Filipowicz, W. (2009). Importance of the C-terminal domain of the human GW182 protein TNRC6C for translational repression. RNA *15*, 781–793.

EXTENDED EXPERIMENTAL PROCEDURES

Cell Culture, Transfection, Plasmid Construction, and Luciferase Assay

C2C12 myoblasts were maintained in Dulbecco's minimal essential medium (DMEM; Life Technology) supplemented with 10% FBS (Life Technology). To induce C2C12 cell differentiation, cells were first grown to reach 80%–90% confluency and the growth medium GM was subsequently replaced with the differentiation media DM (DMEM plus 2% horse serum). Phenotypic differentiation was typically observed after 72 to 96 hr of culturing the cell in DM. Induced myotubes were harvested after differentiation for 4 days. HeLa cells were grown in complete DMEM plus 10% FBS.

For transfection, cells were seeded in 6-well plates and transfected using Lipofectamine 2000 (Life Technology) or TurboFect (Thermo Scientific) after cells reach 50%∼60% confluency. For transfection with siRNAs and miRNAs, Lipofectamine RNAiMAX (Life Technology) was used according to manufacturer's instruction. Briefly, RNA and RNAiMAX were diluted in Opti-MEM and incubated for 15 min. During this interval, cells were seeded in 24-well plates, and the transfection mix was added to the culture media. After 48 hr, cells were harvested with Trizol for RT-PCR or SDS-loading buffer for western.

Su9 (subunit 9 of the F0 ATPase) were amplified from a plasmid containing the gene and inserted in pcDNA3-HA-Ago2 before the HA tag. Plasmids for luciferase reporter assays were constructed by inserting target sequences into the psiCheck2 vector (Promega). The reporter was transfected into cells that had been prior treated with control RNA or miRNAs for 12 hr. Dual luciferase assays were performed 48 hr after plasmid transfection using the luciferase assay kit from Promega. Standard derivation was based on triplicated experiments.

Trypsin/Nuclease Protection Assays

For Trypsin protection assays, isolated mitochondria were split into two aliquots and purified mitoplasts into three aliquots. The first aliquot was kept on ice as control; the second aliquot was treated with Trypsin (100 μg/ml), and the third aliquot of mitoplasts was treated with Trypsin (100 μg/ml) plus Triton X-100 (1%). Treated mitochondria or mitoplasts were collected by centrifugation at 18,000 g for 3 min and the pellets were re-suspended in SDS-PAGE sample buffer for western blotting.

For the nuclease protection assay, isolated mitochondria and mitoplasts were subjected to RNase T1 (3000 U/ml) plus Micrococcal nuclease (1000 U/ml) digestion on ice for 30 min in the presence or absence of Triton X-100. After the reaction, mitochondria or mitoplasts were pelleted by centrifugation, and RNA was extracted from the pellets with Trizol for RT-qPCR analysis.

CLIP-Seq and Data Analysis

CLIP-seq was performed on C2C12 cells cultured in growth media or after switching to differentiation media for 4 days. The library construction was as previously described (Xue et al., 2009, 2013). Sequenced tags were mapped to the mouse genome (mm10) using Bowtie2 (http://bowtie-bio.sourceforge.net/bowtie2/index.shtml). CIMS analysis was according to a published procedure (Zhang and Darnell, 2011).

Analysis of Mitochondrial Translation by Polysome Profiling

Sucrose gradient sedimentation of mitochondrial ribosome/polysome was carried out as described (Antonicka et al., 2013), with modifications. Briefly, mitochondria initially purified from C2C12 myoblasts or myotubes were suspended in the lysis buffer (260 mM sucrose, 100 mM KCl, 20 mM MgCl2, 10 mM Tris-pH 7.5, 1% Triton X-100, 5 mM β-mercaptoethanol, and a cocktail of protease inhibitors from Roche) on ice for 20 min. The lysate was centrifuged at 9,000 g for 30 min to remove particles, loaded on a 8 ml 10%–30% sucrose gradient, and centrifuged at 180,000 g for 260 min in a Beckman SW41-Ti rotor. To characterize the putative polysome, the lysate was pretreated with 5 U/μl RNase I for 40 min at 25°C. After centrifugation, 13 fractions were collected for analysis of RNA and proteins.

Detection of Nascent Protein Synthesis

Click-iT reagents (Life Technology) were used to label nascent polypeptides. C2C12 myoblasts were first transfected with miR-1 or control RNA at 30%–40% confluence in 24-well plates. After culturing overnight, the plate was washed 3 times with prewarmed PBS. The cells were incubated in methionine-free DMEM for 45 min followed by the addition of 20 μM of Emetine, and incubated for another 15 min. The media were replaced with methionine-free DMEM containing 50 μM methionine analog AHA and 20 μM Emetine. After incubation for 4 hr, AHA-containing nascent proteins were labeled with TAMRA (Life Technology), as described (Roche et al., 2009). Labeled proteins were separated in 4%–12% gradient SDS-PAGE and analyzed by Typhoon 9400. The gel was also subjected to western blotting for VDAC and beta actin as loading controls.

Antibodies and Immunocytochemistry

Immunoblotting, immunostaining and immunoprecipitation were performed according to standard procedures using antibodies against COX1 (Abcam, MitoSciences), ND1 (Abcam, PTGlab), beta-actin (Sigma), COX2 (Santa Cruz), COX4 (Santa Cruz), Myogenin (Santa Cruz), Ago2 (Abnova), GW182 (Santa Cruz), Lamin A/C (Santa Crutz), Tom20 (PTGlab), MHC (DSHB), HDAC4 (PTGlab), ELL2 (PTGlab), Pan-actin (Cell Signaling Technology), VDAC (Cell Signaling Technology), Tfam (PTGlab), TACO1 (PTGlab), TNRC6B

(Abnova), TNRC6C (Abnova), ERp72 (PTGlab), ERp60 (PTGlab), Histone H3 (Abcam), Tim23 (PTGlab), Hand2 (Abcam), MRPL24 (Abclonal), MRPS27 (Abclonal), HSP60 (PTGlab) and NDUFB8 (Santa Cruz).

For immunostainning, C2C12 cells were seeded in 12-well plates, fixed with 4% paraformaldehyde for 10 min at room temperature, washed twice with PBS, and then permeabilized for 15 min on ice with 0.1% Triton X-100 in PBS. Cells were washed 3 times with PBS. Primary antibody diluted in PBS containing 3% BSA was applied to the cell and incubated at 4°C overnight. After washing 5 times with PBS, Fluorescent-conjugated secondary antibody was applied to the coverslip and incubated in dark room for 1 hr. At this time, DAPI was applied at proper dilution, and after washing 5 times with PBS, cells were subjected to fluorescent microscopy.

Synthetic RNA, RT-PCR, Quantitative PCR, and Northern Blotting

Control and miR-1 mimics were synthesized as described (Lim et al., 2005). Specific miRNAs and siRNAs used in the study are listed in Table S3. For PCR analysis, total RNA was extracted from cultured cells with Trizol (Life Technology). Complementary DNA was synthesized using 5 μg of total RNA and the ImProme-II reverse transcription system from Promega. Gene-specific primers plus random primers (N9) were used in reverse transcription. The sequences of the forward and reverse primers for PCR are listed in Table S4. RT-qPCR was performed with the Master SYBR Green Kit (Toyobo) on the Rotor Gene 6000 Real-time Analyzer. GAPDH and 18S rRNA served as internal controls. Northern blotting was performed as described (Chen et al., 2006).

miRACE

Two 150 mm dishes of C2C12 cells were induced into myotubes at day 4. Cells were washed 3 times with cold PBS before harvest, scraped from the plates, and collected by centrifugation at 300 g for 5 min. Collected cells were washed once with PBS and treated with wash buffer (0.1% SDS, 0.5% deoxycholate and 0.5% NP-40 in PBS) on ice for 10 min. 500 U DNase I was added and the reaction incubated at 37°C for 5 min. Cell lysate was clarified by centrifugation at 12,000 g for 20 min at 4°C.

The supernatant was used for IP with Ago2 antibody (Abnova) coupled on Protein G Dynal beads (Life Technology). After continuous rotation at 4°C for 2 hr, the supernatant was removed and beads were washed 3 times with wash buffer, twice with high-salt wash buffer (0.1% SDS, 0.5% deoxycholate and 0.5% NP-40 in 5 × PBS), and finally twice with 1 × PNK buffer (50 mM Tris-HCl pH 7.4, 10 mM $MgCl_2$, 0.5% NP-40). The Superscript III reverse transcriptase mix (12 μl RT buffer, 3 μl DTT, 3 μl 10 mM dNTP mix, and 3 μl Superscript III) was added to the beads, and the reaction was incubated at 37°C for 90 min (with rotation at 1,000 rpm for 15 s every 10 min on an Eppendorf thermomixer). Beads were washed twice with the PNK buffer. Poly(C) was added to nascent cDNA by using the TdT mix (44 μl DEPC H_2O, 12 μl tailing buffer, 3 μl 2 mM dCTP, and 1 μl TdT) and the reaction was incubated at 37°C for 30 min. The cDNA-miRNA chimeric molecules were isolated by phenol-chloroform extraction and amplified by PCR using a poly(G) primer and a primer complementary to miR-1. The PCR products of 100 to 200 bp in length were gel purified and cloned into the pMD-18T vector for Sanger sequencing.

Isolation of Mitochondria and Purification of Mitoplasts

Cardiomyocytes from mouse heart, C2C12-derived myoblasts or myotubes were collected by centrifugation and re-suspended in ice-cold isolation buffer (250 mM Sucrose, 10 mM Tris-HCl pH7.4, 1 mM EDTA). The cells were homogenized by 40 to 50 strokes in a prechilled Dounce homogenizer (Kontes). Homogenized samples were centrifuged twice at 800 g for 10 min to collect postnuclear supernatant. Mitochondria were sedimented at 13,000 g for 10 min, washed once in the same buffer, and further purified by centrifugation at 40,000 g for 1 hr at 4°C on a discontinous sucrose (17%, 31%, 42%, 50%) gradient in TE buffer (10 mM Tris-HCl pH 7.4, 20 mM EDTA).

Purification of mitoplasts was according to the procedure as described (Schnaitman and Greenawalt, 1968). Briefly, stock digitonin (10 mg/ml; Sigma) solution at −20°C was diluted to 0.5 mg/ml with isolation buffer, which was used to suspend the mitochondria pellet. After digitonin treatment on ice for 10 min, 4∼5 volumes of isolation buffer were added to the reaction, and the mitochondria were pelleted by centrifugation at 18,000 g at 4°C for 3 min. The pellet was further washed 3 times with 10 volumes of isolation buffer to eliminate soluble outer membrane-associated proteins. The final pellet was designated as mitoplasts. We also further purified mitoplasts by centrifugation on a discontinuous sucrose gradient. In this procedure, digitonin-treated mitochondria were re-suspended in isolation buffer and then layered onto a discontinuous sucrose gradient consisting of 25.2%, 37.7%, 51.1%, and 61.5% layers followed by centrifugation at 77,000 g for 90 min at 4°C. Western blotting analysis of mitochondrial outer and inner membrane proteins indicate that direct sedimentation and purification through the sucrose gradient produced identical results.

Ago2 RIP assay

For ribo-IP experiments, purified mitoplasts from mouse heart was lysed in wash buffer (0.1% SDS, 0.5% deoxycholate and 0.5% NP-40 in PBS) on ice for 15 min followed by treatment with DNase I (Promega) at the final concentration of 500 U/200 μl at 37°C for 10 min. The supernatant was clarified by centrifugation at 12,000 g for 20 min and 200 μl of mitochondrial lysate was added to 50μL Dynal beads (Life Technology) either coupled with 2μg anti-Ago2 antibody or control IgG. After rotation at 4°C for 2 hr, the beads were pelleted; the supernatant removed, and the beads were washed 6 times with wash buffer and twice with high-salt wash buffer (0.1% SDS, 0.5% deoxycholate and 0.5% NP-40 in 5 × PBS). RNA was extracted using Trizol (Life Technology) and analyzed by real-time RT-PCR.

Quantification of Ago2, miR-1, and mtDNA

The relative mtDNA copy number was calculated as a ratio of mtDNA/nuclear (n) DNA according to a previous study (Duchêne et al., 2009). Cells were lysed in the RIPA buffer and DNA extracted with phenol/chloroform followed by ethanol precipitation. For quantification of mtDNA, we used a pair of primers (mtDNA forward, 5′-CCTATCACCCTTGCCATCAT-3′ and mtDNA reverse, 5′-GAGGCTGTTGCTTGTGTGAC-3′) that target the COX1 gene for qPCR analysis. To quantify nDNA, we used a pair of primers (nDNA forward, 5′-ATGGAAAGCCTGCCATCATG-3′ and nDNA reverse, 5′-TCCTTGTTGTTCAGCATCAC-3′) that target the nuclear Pecam gene for qPCR analysis.

His-tagged recombinant Ago2 protein (>95% purity; Sino Biological) was used to generate a standard curve by western blotting. Whole-cell lysate from C2C12 myoblasts or myotubes and lysate of Trypsin-treated mitoplasts were similarly analyzed. The copy number of Ago2 was determined by using the TotalLab quantification program. To quantify the copy number of miR-1 in C2C12 cells before and after differentiation or in purified mitoplasts, we generated a standard curve by RT-qPCR using serially diluted synthetic miR-1 (Ribo Bio) and then performed quantitative analysis of miR-1 in whole-cell lysate or purified mitoplasts.

To determine the copy number of Ago2 or miR-1 per nucleus or per mitochondrial genome, we generated a standard curve by qPCR against a 600 bp nuclear DNA (Pecam) and 1,544 bp (full length) COX1 DNA, respectively. We used these standard curves to calculate the copy number of Ago2 and miR-1 based on western blotting or RT-qPCR analysis performed on the same batch of Trypsin-treated mitoplasts and total cell lysate.

Measurement of Mitochondrial Activities

The ATP assay kit was from Beyotime and the assay was performed according to manufacturer's instruction. After centrifugation to remove cell debris, the supernatant was added to the substrate solution. The luminescence was recorded in an Illuminometer with an integration time of 10 s per well.

The activity of NADH-ubiquinone oxidoreductase (Complex I) was assayed as described (Frost et al., 2005). Briefly, isolated mitochondria were frozen and thawed to cause gentle opening. The mix was added to a 10 mM potassium phosphate buffer (pH 8.0) containing 1 μM antimycin A and 0.2 mM NADH). The rate of NADH oxidation was followed at 340 nm in a UV spectrophotometer (Bio-Rad). After absorbance was recorded for 1 min, ubiquinone was added at the final concentration of 70 μM, and the stimulated rate of NADH oxidation (Complex I activity) was followed for another 2 min. The Complex I activity was calculated from the slope of absorbance decrease over time using an extinction coefficient for NADH. The cytochrome c oxidase activity (Complex IV) was assayed by measuring oxidation of cytochrome c at 550 nm using a cytochrome c oxidase activity kit (Genmed).

Determination of Mitochondrial Protein Stability

To determine the stability of mitochondrial proteins, the mitochondrial translation inhibitor Chloramphenicol INN (50 μg/ml) was included in the culture media for control RNA or miR-1 transfected C2C12 cells. Whole-cell lysate was obtained at different time points (0 min, 2 hr, 4 hr, 8 hr, 16 hr, 32 hr), fractionated by 12% SDS-PAGE and subjected to western blotting for ND1 and Actin. The western blotting signals were quantified by using the program from TotalLab and the levels of ND1 were compared against that at the 0 min treatment point.

SUPPLEMENTAL REFERENCES

Duchêne, A.M., Pujol, C., and Maréchal-Drouard, L. (2009). Import of tRNAs and aminoacyl-tRNA synthetases into mitochondria. Curr. Genet. *55*, 1–18.

Frost, M.T., Wang, Q., Moncada, S., and Singer, M. (2005). Hypoxia accelerates nitric oxide-dependent inhibition of mitochondrial complex I in activated macrophages. Am. J. Physiol. Regul. Integr. Comp. Physiol. *288*, R394–R400.

Lim, L.P., Lau, N.C., Garrett-Engele, P., Grimson, A., Schelter, J.M., Castle, J., Bartel, D.P., Linsley, P.S., and Johnson, J.M. (2005). Microarray analysis shows that some microRNAs downregulate large numbers of target mRNAs. Nature *433*, 769–773.

Roche, F.K., Marsick, B.M., and Letourneau, P.C. (2009). Protein synthesis in distal axons is not required for growth cone responses to guidance cues. J. Neurosci. *29*, 638–652.

Xue, Y., Zhou, Y., Wu, T., Zhu, T., Ji, X., Kwon, Y.S., Zhang, C., Yeo, G., Black, D.L., Sun, H., et al. (2009). Genome-wide analysis of PTB-RNA interactions reveals a strategy used by the general splicing repressor to modulate exon inclusion or skipping. Mol. Cell *36*, 996–1006.

Xue, Y., Ouyang, K., Huang, J., Zhou, Y., Ouyang, H., Li, H., Wang, G., Wu, Q., Wei, C., Bi, Y., et al. (2013). Direct conversion of fibroblasts to neurons by reprogramming PTB-regulated microRNA circuits. Cell *152*, 82–96.

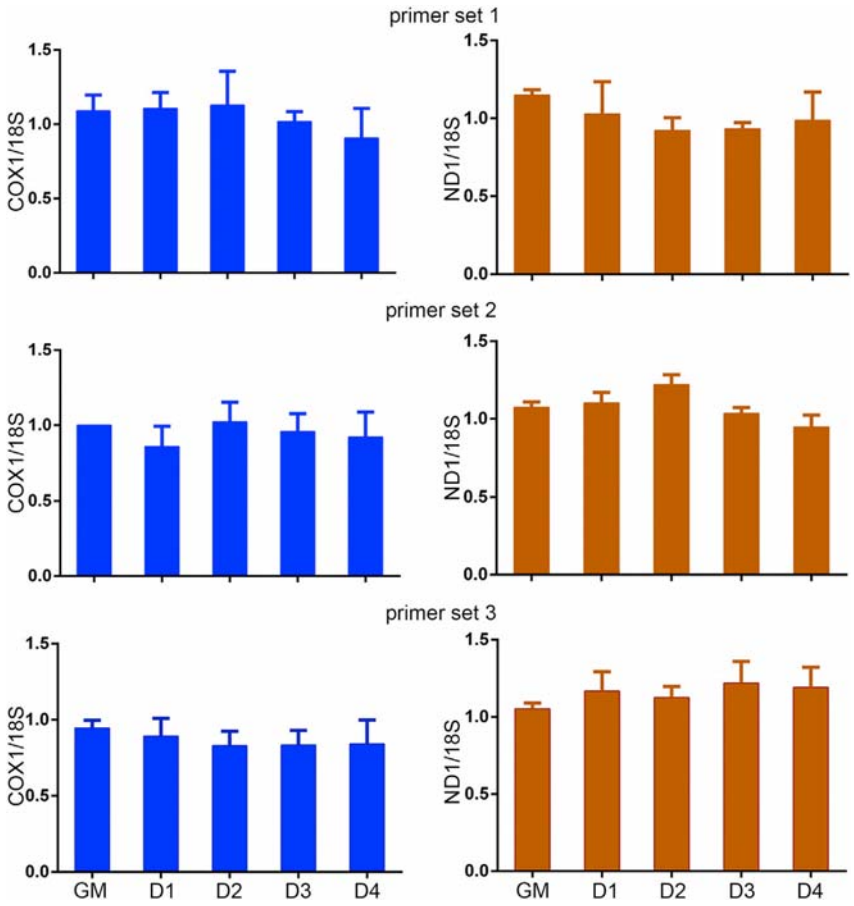

Figure S1. Quantitative Analysis of the mRNA Levels of COX1 and ND1 during C2C12 Myogenesis with Three Distinct Primer Sets against Each Transcript, Related to Figure 1

Total RNAs were extracted from C2C12 cells in growth media (GM) or after switching to differentiation media for days (D) indicated. The mitochondrial transcripts COX1 and ND1 were quantified by RT-qPCR with three separate PCR primers listed in Table S4 and normalized against the levels of the 18S rRNA.

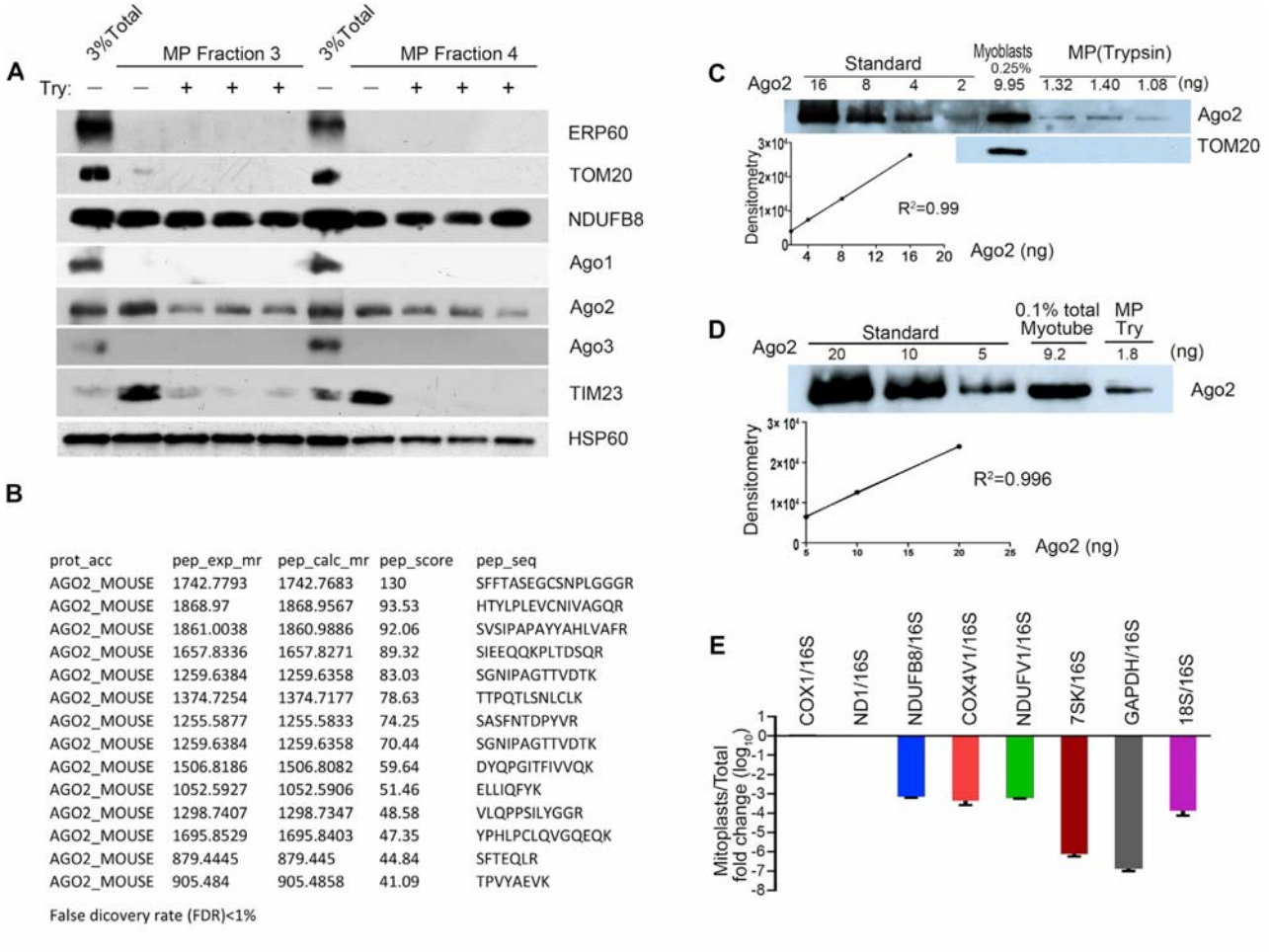

B

prot_acc	pep_exp_mr	pep_calc_mr	pep_score	pep_seq
AGO2_MOUSE	1742.7793	1742.7683	130	SFFTASEGCSNPLGGGR
AGO2_MOUSE	1868.97	1868.9567	93.53	HTYLPLEVCNIVAGQR
AGO2_MOUSE	1861.0038	1860.9886	92.06	SVSIPAPAYYAHLVAFR
AGO2_MOUSE	1657.8336	1657.8271	89.32	SIEEQQKPLTDSQR
AGO2_MOUSE	1259.6384	1259.6358	83.03	SGNIPAGTTVDTK
AGO2_MOUSE	1374.7254	1374.7177	78.63	TTPQTLSNLCLK
AGO2_MOUSE	1255.5877	1255.5833	74.25	SASFNTDPYVR
AGO2_MOUSE	1259.6384	1259.6358	70.44	SGNIPAGTTVDTK
AGO2_MOUSE	1506.8186	1506.8082	59.64	DYQPGITFIVVQK
AGO2_MOUSE	1052.5927	1052.5906	51.46	ELLIQFYK
AGO2_MOUSE	1298.7407	1298.7347	48.58	VLQPPSILYGGR
AGO2_MOUSE	1695.8529	1695.8403	47.35	YPHLPCLQVGQEQK
AGO2_MOUSE	879.4445	879.445	44.84	SFTEQLR
AGO2_MOUSE	905.484	905.4858	41.09	TPVYAEVK

False dicovery rate (FDR)<1%

F

Ago2 IP/Input in Mitoplasts

miR-1	COX1	COX2	COX3	ND1	ND2	ND3	ND4	ND4L	ND5	ND6	cyt b	ATP6	ATP8
380.8	22.3	<1	<1	47.8	24.1	<1	<1	41.1	8.2	<1	31.8	2.8	<1

Figure S2. The Characterization and Quantification of Ago2 in the Mitochondria, Related to Figure 2

(A) The Trypsin protection assay performed on individual sucrose gradient fractions (3 and 4) containing mitoplasts purified from mouse heart.

(B) Results of tandem mass spectrometric analysis of Ago2 immunoprecipitated from mouse heart mitoplasts.

(C and D) Standard curves generated with baculovirus-expressed Ago2 for quantification of Ago2 in whole-cell lysate and purified mitoplasts from C2C12 myoblasts and myotubes.

(E) Evaluation of residual levels of nonmitochondrial mRNAs on purified mitoplasts relative to mitochondrial 16S rRNA. In comparison with the 1:1 ratio of COX1:16S rRNA and ND1:16S rRNA (thus the log10 ratio = 0 in both cases), the results indicate that all nonmitochondrial mRNAs, including those encoding for mitochondrial proteins, such as NDUFB8, COX4V1, and NDUFV1, were reduced by at least 3 orders of magnitude.

(F) Quantification of Ago2 associated mtDNA-encoded transcripts by real-time RT-PCR in purified mitoplasts. The results were presented as the percentage of each specific mRNA in Ago2 immunoprecipitant versus input from mitoplasts.

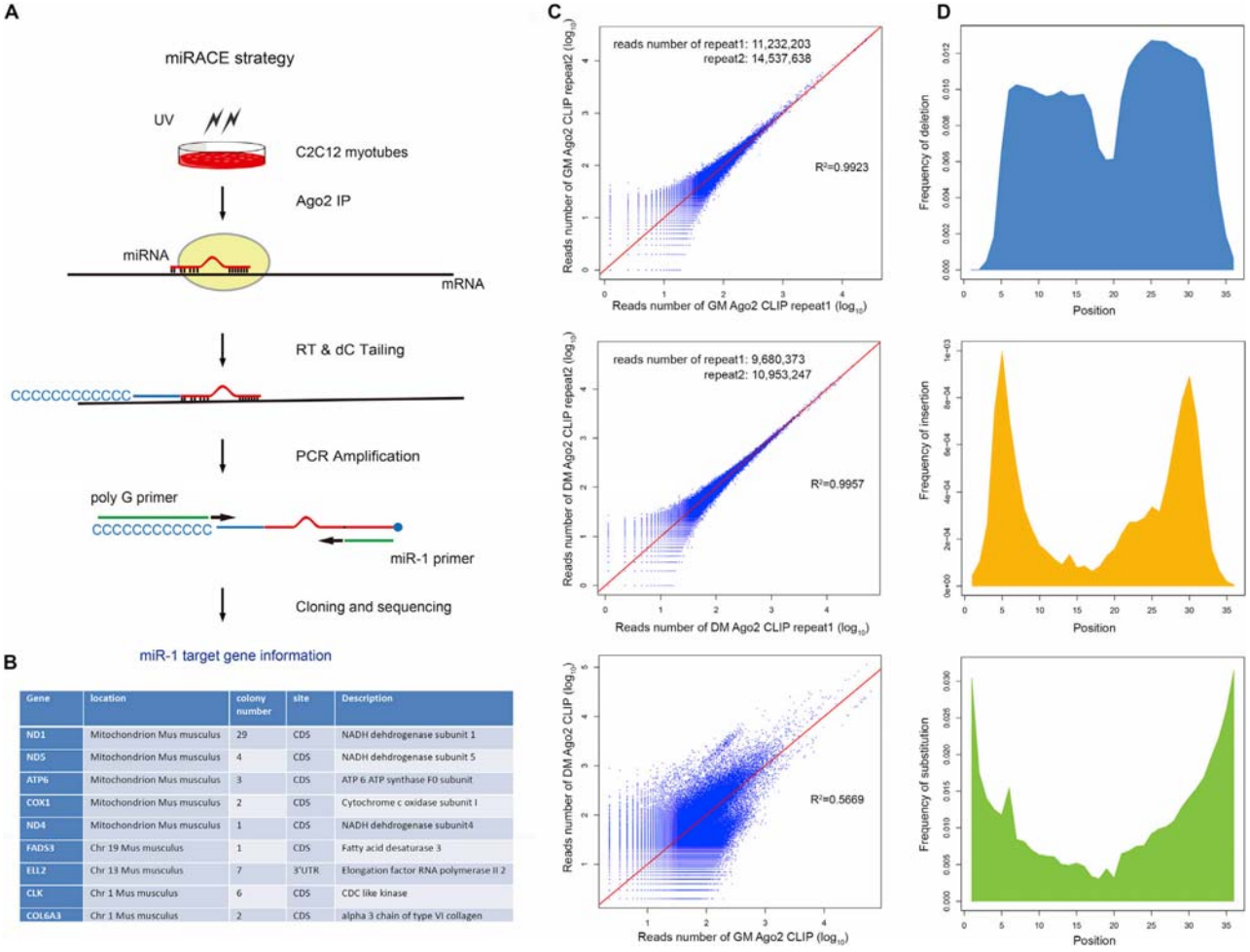

Gene	location	colony number	site	Description
ND1	Mitochondrion Mus musculus	29	CDS	NADH dehdrogenase subunit 1
ND5	Mitochondrion Mus musculus	4	CDS	NADH dehdrogenase subunit 5
ATP6	Mitochondrion Mus musculus	3	CDS	ATP 6 ATP synthase F0 subunit
COX1	Mitochondrion Mus musculus	2	CDS	Cytochrome c oxidase subunit I
ND4	Mitochondrion Mus musculus	1	CDS	NADH dehdrogenase subunit4
FADS3	Chr 19 Mus musculus	1	CDS	Fatty acid desaturase 3
ELL2	Chr 13 Mus musculus	7	3'UTR	Elongation factor RNA polymerase II 2
CLK	Chr 1 Mus musculus	6	CDS	CDC like kinase
COL6A3	Chr 1 Mus musculus	2	CDS	alpha 3 chain of type VI collagen

Figure S3. Illustration of the Experimental Scheme for miRACE and Demonstrating the Robustness of Ago2 CLIP-seq Experiments on C2C12 Myoblasts and Myotubes, Related to Figure 3

(A) The scheme of the miRACE strategy.

(B) Identified miR-1 targets by cloning and sequencing.

(C) The reproducibility of two independent CLIP-seq experiments on C2C12 myoblasts (top) and myotubes (middle), as well as comparison between myoblasts and myotubes based on the combined data sets (bottom).

(D) The frequency and distribution of deletions (top), insertions (middle) and substitutions (bottom) in the Ago2 CLIP-seq tags mapped to mtDNA-encoded transcripts.

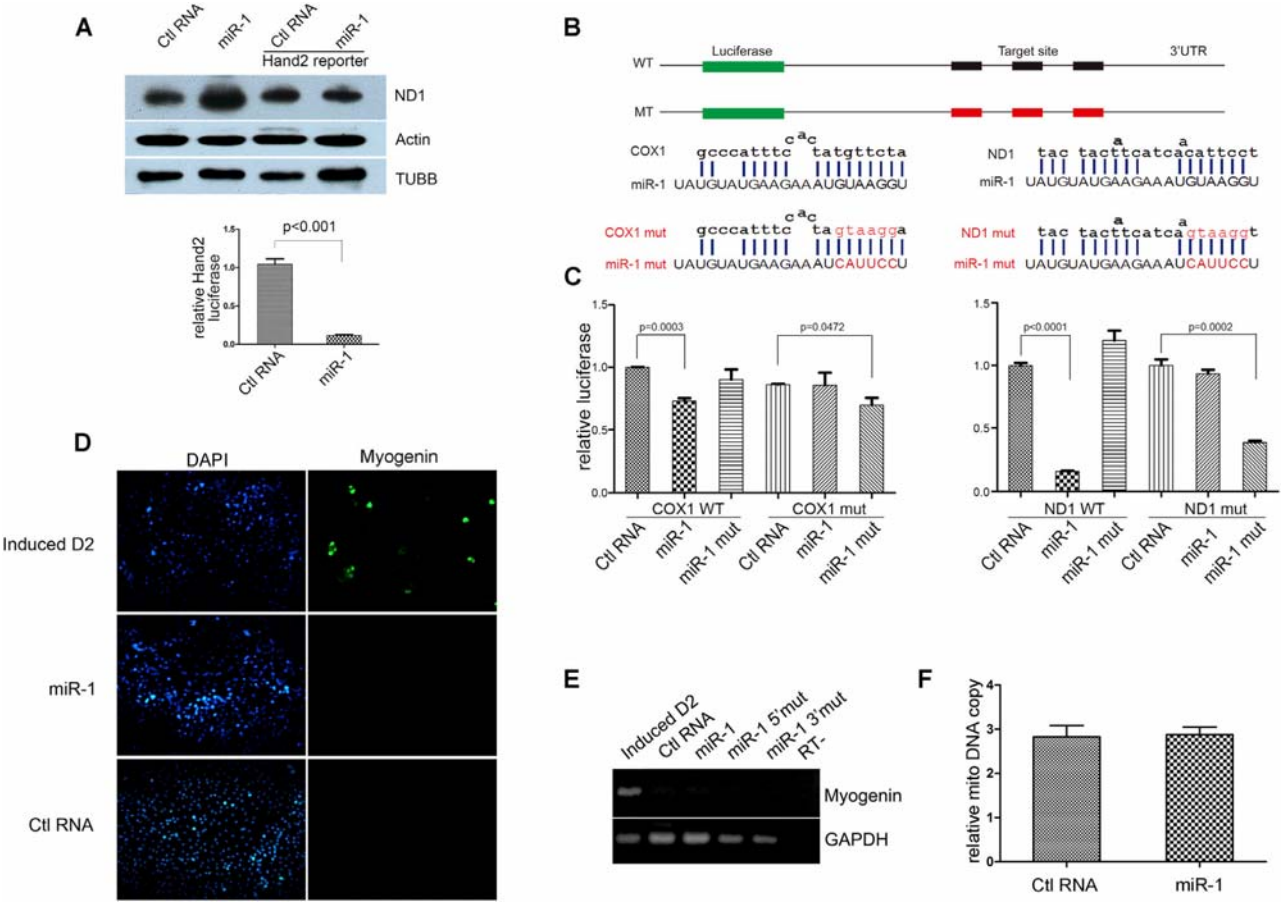

Figure S4. A Series of Supporting Evidence for the Direct Effect of miR-1 in Enhancing Mitochondrial Translation, Rather than due to Indirectly Induced Myogenic Program, Related to Figure 4

(A) Prevention of miR-1 mediated translational enhancement by a cytoplasmic sponge expressed from a Hand2-based reporter.

(B and C) miR-1 repressed the cytoplasmic reporter containing three miR-1 target sites from ND1 and COX1. The mutant miR-1 site in the reporter lost the effect, which could be restored with the corresponding mutant miR-1 that reestablished the required base-pairing interactions.

(D and E) Transfected miR-1 alone was insufficient to induce the myogenic program on C2C12 cells.

(F) No change in mtDNA copy number in miR-1 transfected C2C12 cells.

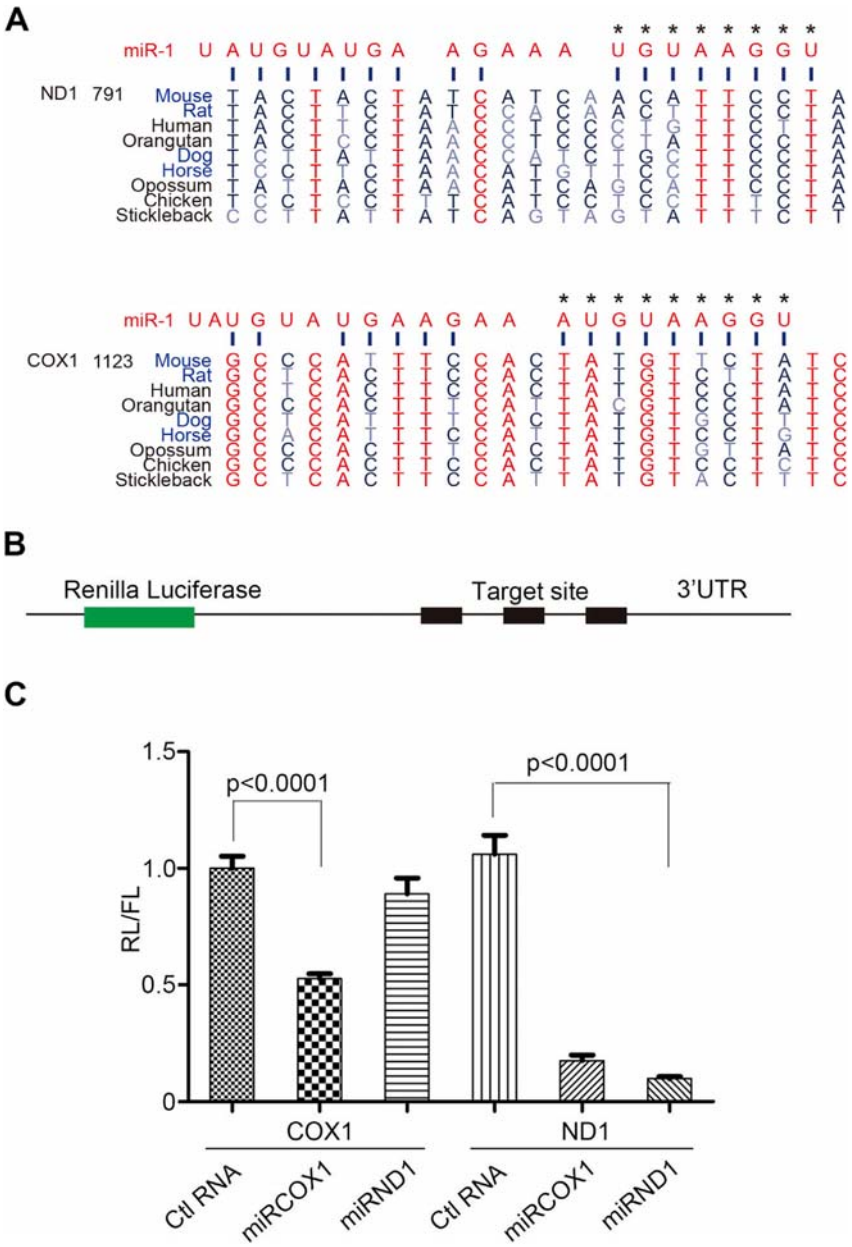

Figure S5. The Evolutionary Conservation of miR-1 Target Sites in ND1 and COX1 and Luciferase Reporter Assays to Characterize miR-1 Target Sites in the Cytoplasm, Related to Figure 5

(A) Evolutionary conservation of miR-1 target sites in ND1 and COX1. Red-labeled nucleotides have base-pairing potential with miR-1.

(B and C) The designer miRND1 and miRCOX1 were effective in repressing the corresponding luciferase reporters in the cytoplasm. Note a level of partial effect of miRCOX1 on ND1 reporter because of the reduced, but not abolished base-pairing in the seed region of both COX1 and ND1 target sites in the reporters.